Structure of the membrane proximal external region of HIV-1 envelope glycoprotein

Qingshan Fu[a,1], Md Munan Shaik[b,c,1], Yongfei Cai[b,c], Fadi Ghantous[d], Alessandro Piai[a], Hanqin Peng[b], Sophia Rits-Volloch[b], Zhijun Liu[e], Stephen C. Harrison[a,b,c,2], Michael S. Seaman[d], Bing Chen[b,c,2], and James J. Chou[a,e,2]

[a]Department of Biological Chemistry and Molecular Pharmacology, Harvard Medical School, Boston, MA 02115; [b]Division of Molecular Medicine, Boston Children's Hospital, Harvard Medical School, Boston, MA 02115; [c]Department of Pediatrics, Harvard Medical School, Boston, MA 02115; [d]Center for Virology and Vaccine Research, Beth Israel Deaconess Medical Center, Boston, MA 02215; and [e]State Key Laboratory of Molecular Biology, National Center for Protein Science Shanghai, Shanghai Science Research Center, Shanghai Institute of Biochemistry and Cell Biology, Chinese Academy of Sciences, 201203 Shanghai, China

Contributed by Stephen C. Harrison, August 2, 2018 (sent for review April 26, 2018; reviewed by Peter S. Kim and Michael F. Summers)

The membrane-proximal external region (MPER) of the HIV-1 envelope glycoprotein (Env) bears epitopes of broadly neutralizing antibodies (bnAbs) from infected individuals; it is thus a potential vaccine target. We report an NMR structure of the MPER and its adjacent transmembrane domain in bicelles that mimic a lipid-bilayer membrane. The MPER lies largely outside the lipid bilayer. It folds into a threefold cluster, stabilized mainly by conserved hydrophobic residues and potentially by interaction with phospholipid headgroups. Antigenic analysis and comparison with published images from electron cryotomography of HIV-1 Env on the virion surface suggest that the structure may represent a prefusion conformation of the MPER, distinct from the fusion-intermediate state targeted by several well-studied bnAbs. Very slow bnAb binding indicates that infrequent fluctuations of the MPER structure give these antibodies occasional access to alternative conformations of MPER epitopes. Mutations in the MPER not only impede membrane fusion but also influence presentation of bnAb epitopes in other regions. These results suggest strategies for developing MPER-based vaccine candidates.

HIV-1 Env | membrane proximal region | NMR structure | transmembrane region

HIV-1 Env [trimeric $(gp160)_3$, cleaved to $(gp120/gp41)_3$], the sole antigen on the virion surface, induces strong antibody responses in infected individuals (1, 2). Env directs fusion of viral and host-cell membranes to initiate infection of a susceptible cell (3). Conformational changes accompany binding of the native Env trimer to receptor (CD4) and coreceptor (e.g., CCR5 or CXCR4), leading to a cascade of refolding events in gp41 (*SI Appendix*, Fig. S1*A*). The N-terminal fusion peptide of gp41 inserts into the target cell membrane, forming an extended conformation known as a "prehairpin intermediate" (4). Subsequent folding back of the C-terminal region of gp41 into a hairpin conformation creates the postfusion, six-helix bundle (5, 6), bringing together viral and cellular membranes to induce fusion and viral entry.

A ∼24-residue hydrophobic region (residues 660–683), immediately preceding the transmembrane domain (TMD) and known as the membrane-proximal external region (MPER), is one of the most conserved regions in gp41 (*SI Appendix*, Fig. S1*B*). The MPER, required for infectivity (7–9), is the epitope for several well-characterized broadly neutralizing antibodies (bnAbs) (10–13). MPER structures have been studied extensively by both NMR and X-ray crystallography under a wide range of conditions. It tends to adopt an α-helical conformation with or without a break in the middle. For example, a monomeric MPER peptide examined by NMR in detergent micelles folded into a kinked helix with many hydrophobic residues embedded in the micelles (14, 15). This result has led to a widely held belief that the MPER should be buried in viral membrane. Conversely, in the postfusion conformation of soluble gp41 trimer, the MPER forms a continuous helix (16–18). It is disordered in a cryo-EM structure of a detergent-solubilized clade B JR-FL EnvΔCT construct containing both the MPER and TMD (19), perhaps because of effects of the detergent micelle.

The MPER is the target of several anti-gp41 bnAbs, including 2F5, 4E10, and 10E8 (10–12). When liganded by bnAbs, the C-terminal half of the MPER retains its helical conformation, but its N-terminal half can adopt extended, nonhelical structures (13, 20–23), consistent with its conformational plasticity during membrane fusion. The MPER-directed bnAbs often contain a long heavy-chain third complementarity-determining region (HCDR3), with a hydrophobic surface, essential for neutralizing activity, that does not make direct contacts with gp41 but interacts instead with the membrane (24, 25). From the structure of an MPER peptide embedded in a detergent micelle, it has been proposed that these antibodies extract their epitopes out of the viral membrane (14, 15, 26). Other evidence suggests instead that these antibodies block HIV-1 infection by recognizing the prehairpin intermediate conformation of gp41 with the help of their lipid binding activity (22–24, 27, 28). Recent structural studies have shown that phospholipids may indeed be an integral component of the epitopes, at least, for 4E10 and 10E8 (22, 23). In

Significance

The conserved, membrane-proximal external region (MPER) of the HIV-1 envelope glycoprotein (Env) is a potential vaccine target. To visualize its structure in the context of a lipid-bilayer membrane, we have reconstituted a polypeptide containing the HIV-1 MPER and the contiguous transmembrane domain into a bilayer-like environment and determined its atomic structure by NMR. The MPER folds into a trimeric cluster, well exposed on the bilayer surface, even in the absence of the structural constraints from the rest of the Env ectodomain. Our analyses suggest that this structure probably represents a prefusion conformation of the MPER. The findings imply that presenting a well-defined structure will be important for MPER-based immunogen design.

Author contributions: Q.F., M.M.S., Y.C., B.C., and J.J.C. designed research; Q.F., M.M.S., Y.C., F.G., A.P., H.P., S.R.-V., and Z.L. performed research; M.S.S. contributed new reagents/analytic tools; Q.F., M.M.S., Y.C., F.G., A.P., H.P., S.R.-V., S.C.H., M.S.S., B.C., and J.J.C. analyzed data; and Q.F., M.M.S., S.C.H., B.C., and J.J.C. wrote the paper.

Reviewers: P.S.K., Stanford University School of Medicine; and M.F.S., University of Maryland.

The authors declare no conflict of interest.

Data deposition: The atomic structure coordinate and structural constraints have been deposited in the Protein Data Bank, www.wwpdb.org (PDB ID code 6E8W). The chemical shift values have been deposited in the Biological Magnetic Resonance Data Bank, www.bmrb.wisc.edu (accession no. 30503).

[1]Q.F. and M.M.S. contributed equally to this work.

[2]To whom correspondence may be addressed. Email: harrison@crystal.harvard.edu, bchen@crystal.harvard.edu, or james_chou@hms.harvard.edu.

This article contains supporting information online at www.pnas.org/lookup/suppl/doi:10.1073/pnas.1807259115/-/DCSupplemental.

Published online September 5, 2018.

addition to membrane binding, many MPER-targeted bnAbs also show polyreactivity to environmental antigens and/or autoreactivity to self antigens (29–31), raising concerns about how to induce them safely by vaccination.

To define the structure of the HIV-1 MPER under more physiologically relevant conditions than used for previous studies and to guide immunogen design, we have determined by NMR its structure when linked to the Env TMD in the context of a lipid bilayer.

Results

Structure Determination. We previously determined the structure of the TMD reconstituted in bicelles using a fragment of gp41 (residues 677–716) derived from a clade D HIV-1 isolate 92UG024.2 [designated gp41$^{HIV1D(677–716)}$] (32). The TMD forms a tightly assembled trimer stabilized by an N-terminal coiled-coil and a C-terminal hydrophilic core. (We discuss a subsequent challenge to this model at the end of this section.) To define the MPER–TMD structure in the context of a lipid bilayer, we used bicelle reconstitution as developed for the TMD and extended the protein sequence to include the MPER. We identified a gp41 fragment, residues 660–710 (*SI Appendix*, Fig. S1*B*), that had excellent solution NMR properties in dimyristoylphophatidylcholine/dihexanoylphosphatiylcholine (DMPC/DHPC) bicelles with $0.5 \leq q \leq 0.6$ (*SI Appendix*, Fig. S1*C*). This construct, designated gp41$^{HIV1D(660–710)}$ or MPER-TMD, contains the entire MPER (residues 660–683) and TMD (residues 684–705) (33, 34). We purified MPER-TMD and reconstituted it into bicelles with procedures similar to those used for gp41$^{HIV1D(677–716)}$. The mobility of the reconstituted MPER-TMD in SDS/PAGE was close to that expected for a trimer (theoretical molecular weight 18.5 kDa) (*SI Appendix*, Fig. S1*D*), consistent with our earlier observation that the trimer of gp41$^{HIV1D(677–716)}$ resists SDS denaturation (32). We confirmed trimerization of MPER-TMD by cross-linking and urea-PAGE analysis (*SI Appendix*, Fig. S1*E*).

NMR spectra and carbon secondary chemical shifts of the core region of the TMD (residues 685–702) in MPER-TMD are almost identical to those of the same segment in gp41$^{HIV1D(677–716)}$ (*SI Appendix*, Fig. S2 *A–E*), indicating that addition of the MPER did not alter the TMD conformation. This result justified the use during the MPER-TMD structure calculation of NMR-derived structural restraints for residues 685–702, assigned previously for the TMD. These restraints were valuable, because the same region of the MPER-TMD did not generate sufficient NOE data, owing to fast signal relaxation resulting from the larger size of the construct. The regions of MPER-TMD outside the TM core nevertheless showed excellent spectroscopic properties, because of their greater local dynamics, allowing a comprehensive analysis of NOE data. We completed the structure of the MPER-TMD trimer by a strategy similar to the one we had used previously for the TMD alone (32, 35). We first determined the local MPER structures and then measured interprotomer NOEs between structurally equivalent but isotopically differently labeled protomers (*SI Appendix*, Fig. S3*A*). A control analysis of homotrimeric (^{15}N, ^{2}H)-labeled MPER-TMD, prepared from the same labeling batch used for mixing, ensured that NOEs were not due to low levels of ^{1}H in the samples (*SI Appendix*, Fig. S3 *B* and *C*). We also confirmed assignment of intermolecular NOE cross-peaks by selectively detecting NOEs between ^{1}H(^{15}N) of one strand and ^{1}H(^{13}C) of a neighboring strand (*SI Appendix*, Fig. S3*D*). Finally, we showed that those NOE cross-peaks we could detect from the TM core of the MPER-TMD corresponded to strong peaks from the published TM NOE analysis (*SI Appendix*, Fig. S4*A*). The final ensemble of structures converged to rmsd of 1.19 Å and 1.71 Å for backbone and all heavy atoms, respectively (*SI Appendix*, Fig. S4 *B* and *C* and Table S1).

In addition to NOE-based structure determination, we performed paramagnetic relaxation enhancement (PRE) analysis of a mixed sample, in which half of the MPER-TMDs were spin-labeled at either the N terminus (L660) or the C terminus (Q710) and the other half ^{15}N-labeled. If the MPER-TMD forms oligomers, the NMR resonances of the relevant region will show strong PRE. With the N-terminal spin label, our measurements showed strong PRE in the N-terminal helix (residues 660–672), with an average signal loss of ∼50% (*SI Appendix*, Fig. S5*A*), as expected from 1:1 random mixing of spin-labeled and unlabeled protomers. In contrast, the TMD, which is far from the spin label, was unaffected. Furthermore, L663 and A667, the two residues closest to the N terminus of the neighboring protomer in our NMR structure, showed the strongest PRE (*SI Appendix*, Fig. S5*A*), offering further validation of the calculated model. We obtained the converse result—strong PRE in the TM region and none in the MPER—with the C-terminal spin label (*SI Appendix*, Fig. S5*B*). In that case, L704 showed the strongest PRE. C-terminal spin labeling of the TMD alone (a construct that extended to residue 716) resulted in strong PRE for residues near the C terminus of the ^{15}N-labeled chain (*SI Appendix*, Fig. S5*C*), including L704. These data show that the TMD C termini lie relatively close together in both constructs.

An NMR study of a bicelle-embedded, TMD construct identical to ours (36) has suggested that this peptide is a monomer tilted with respect to the membrane normal, rather than the trimer we described (32). We have shown here by cross-linking that our MPER-TMD construct is trimeric and by PRE experiments with spin label at either end that there are close trimer interactions at both termini of the fragment. Moreover, the mixed NOE experiment definitively identifies intersubunit NOEs in the MPER-TMD spectra. We have also now carried out the C-terminal spin-label PRE experiment on the TMD fragment, showing that it too is an oligomer. We describe in *SI Appendix* possible sources of the discrepant interpretations, but we believe that the data presented here confirm our previously published interpretation of the TMD structure.

MPER-TMD Structure and Its Transmembrane Partition. The MPER in this trimeric assembly is well-ordered (Fig. 1*A*), showing substantial interchain contacts not expected from any of the previously reported structures (14–16). The MPER folds into two α-helices connected by a sharp turn (Fig. 1*B*). The C-terminal helix (C-helix) connects into the coiled-coil region of the TMD through a kink at K/R683 (Fig. 1*C*). The broken main-chain hydrogen bond(s) at this kink (O^{679}–HN^{683}, and possibly O^{680}–HN^{684}) expose donors and acceptors that could be stabilized by bound water or lipid headgroups. Moreover, the guanidinium group of R683, although not precisely defined by NMR data, could form a hydrogen bond with the backbone oxygen of either L679 or W680 (Fig. 1*C*). The N-terminal helix (N-helix) connects to the C-helix by a ∼90° turn at conserved residues W672 and F673 (Fig. 1*D*). The N-helices from the three protomers converge around the threefold axis and create a hydrophobic core sequestering L661 and W666 (Fig. 1*E*); L669 and W670 appear to extend the hydrophobic core at the periphery. An L669S substitution leads to prolonged exposure of the MPER neutralizing epitopes (37), suggesting that the hydrophobic core is important for maintaining the antigenic structure of prefusion Env. Overall, some of the most conserved residues in this region determine the MPER trimer conformation. The structure can thus explain the strict conservation of these residues, rather than just retention of the hydrophobicity that would be needed for the membrane insertion suggested by others (14, 15).

To position the MPER with respect to the lipid bilayer, we analyzed the transmembrane partition of the MPER-TMD trimer using our previously developed paramagnetic probe titration (PPT) method (38). We reconstituted the MPER-TMD protein in bicelles with $q = 0.6$ and titrated the water-soluble paramagnetic probe Gd-DOTA into the aqueous phase surrounding the bicelles, allowing us to measure residue-specific PRE amplitudes (PRE_{amp}) (Fig. 2*A* and *SI Appendix*, Fig. S6). A plot of PRE_{amp} vs. (residue number) changes slope by ∼30° at R683, between the C-helix of

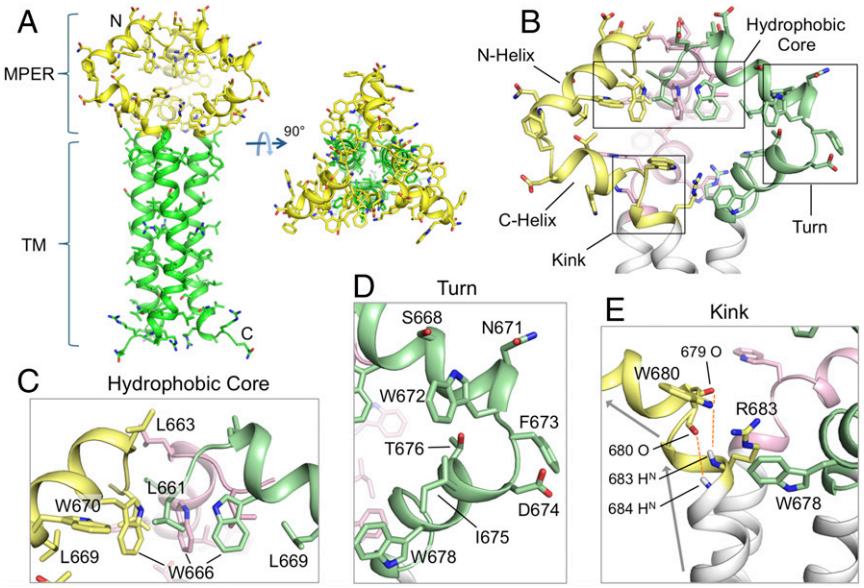

Fig. 1. Structure of the MPER-TMD of HIV-1 Env. (*A*) Ribbon representation of the average structure of the calculated ensemble. The MPER (residues 660–683) and the TMD (residues 684–710) are shown in yellow and green, respectively. (*B*) A close-up view of the MPER trimer showing the three protomers in different colors, as well as the characteristic features including the N- and C-helices, the hydrophobic core, the turn connecting the N- and C-helices, and the kink between the C-helix and TMD. (*C*) The "hydrophobic core" consisting of N-helix hydrophobic residues (W666, W670, L661, and L669). (*D*) The "turn" region containing residues 671–676. (*E*) The "kink" at residues 680–683 resulting in a ∼45° change in helix orientation (indicated by the arrows). The O(i)–HN(i + 4) distances of 679–683 and 680–684, indicated by red dashed lines, are >5 Å, much greater than a standard hydrogen bond distance (∼2.5 Å).

MPER and the N-terminal portion of the TM helix (Fig. 2*A*); this change provides independent evidence for the kink in the calculated NMR structure (Fig. 1*C*). The PRE_{amp} is flat at value ∼1.0 for the N-helix of MPER, indicating that this helical segment is completely solvent-exposed. To position the MPER-TMD relative to the bilayer, we calculated, for each residue, the distance along the protein symmetry axis (r_z), assumed normal to the bilayer, from the amide proton to an arbitrary reference point. This calculation converted PRE_{amp} vs. (residue number) to PRE_{amp} vs. r_z, which we then analyzed by sigmoidal fitting (*Materials and Methods*) to position the structure relative to the bilayer center (Fig. 2*B*). The results indicate that part of the C-helix lies in the lipid headgroup region, while the rest of the MPER lies outside the membrane (Fig. 2*C*). In particular, none of the conserved hydrophobic residues in the MPER is submerged in the hydrophobic part of the lipid bilayer.

We docked the MPER-TMD structure into low-resolution density, derived from cryo-electron tomography (cryo-ET), of unliganded, prefusion Env trimer on the surface of HIV-1 virions (39). When placed according to the PRE-derived TMD position in the viral membrane (Fig. 2*D*), the MPER matches a triangle-shaped density that bridges the gap between the docked model of an SOSIP.664 trimer (40–43), which terminates just at the N-terminal end of the MPER, and the viral membrane. Thus, the MPER conformation we see by NMR is consistent with the structure of prefusion Env on the virion. The published gp140 SOSIP structures extend, as a C-terminal helix, to residue 664 and hence overlap very slightly the sequence included in our MPER construct. A cryo-EM structure that includes the MPER and TM (5FUU) (19) becomes disordered at residue 656, however, suggesting that residues 656–660 may depart from the helical structure seen in the truncated constructs. We therefore cannot make any conclusions about how the major part of the ectodomain would connect to the MPER in the structure we have determined.

Antigenic Properties of the MPER-TMD. Many known MPER-specific bnAbs, such as 2F5, 4E10, and 10E8, do not bind the prefusion Env trimer; they neutralize primarily by targeting the receptor-bound conformation (24, 27, 28). The 2F5 epitope has an α-helical conformation in the MPER-TMD trimer (Fig. 3*A*) incompatible with 2F5 binding (20). Likewise, when the structures of 4E10 and 10E8 in complex with their epitope peptides are superposed on the MPER-TMD structure, both antibodies overlap with other parts of the trimer (Fig. 3*A*). A weakly neutralizing antibody, DH570 (44), elicited by vaccination of rhesus macaques, could bind the MPER-TMD without major hindrance, although optimal binding might require slight rotation of the epitope helix (Fig. 3*A*).

To test the structural modeling experimentally, we determined antibody binding of the bicelle-reconstituted MPER-TMD in solution by monitoring loss of its NMR signals when bound to an antibody. Addition of three antigen-binding fragments (Fabs), a total of ∼150 kDa, should make the MPER-TMD essentially NMR-invisible, due to the increased molecular mass of the antibody complex. When we added the Fab of 2F5, 4E10, or 10E8 to the MPER-TMD at a molar ratio of ∼1.0:0.7, the NMR peak intensity diminished very slowly and steadily over a course of 4–10 h (Fig. 3 *B*–*E*). In contrast, addition of an anti–His-tag Fab (prepared from MA1-21315) to the MPER-TMD bearing an N-terminal 6His-tag led to instant loss of NMR signals (Fig. 3*F*). No obvious changes were detected after addition of an anti-gp120 antibody VRC01 (45), as expected (Fig. 3*G*). These results indicate that the MPER conformation is incompatible with binding of the three MPER bnAbs, as predicted, but that a slow conformational change allows the Fabs to associate. The peak intensities at each time point in Fig. 3 *B*–*F* represent the amount of MPER-TMD in the NMR samples not bound to the Fabs. The plots of (fraction unbound) vs. time are linear (Fig. 3*G*); extrapolation to time 0 determines the fraction of MPER-TMD that cannot readily bind the Fabs. For the 2F5, 4E10, and 10E8 Fabs, although their time dependences show different slopes, the plots extrapolate to ∼90% at time 0, indicating that less than 10% of the MPER-TMD conformation in the NMR sample exposed the relevant epitopes for Fab binding. As expected, over 90% of the His-tagged MPER-TMD is in a conformation compatible with binding to the anti–His-tag Fab. DH570 is an intermediate case;

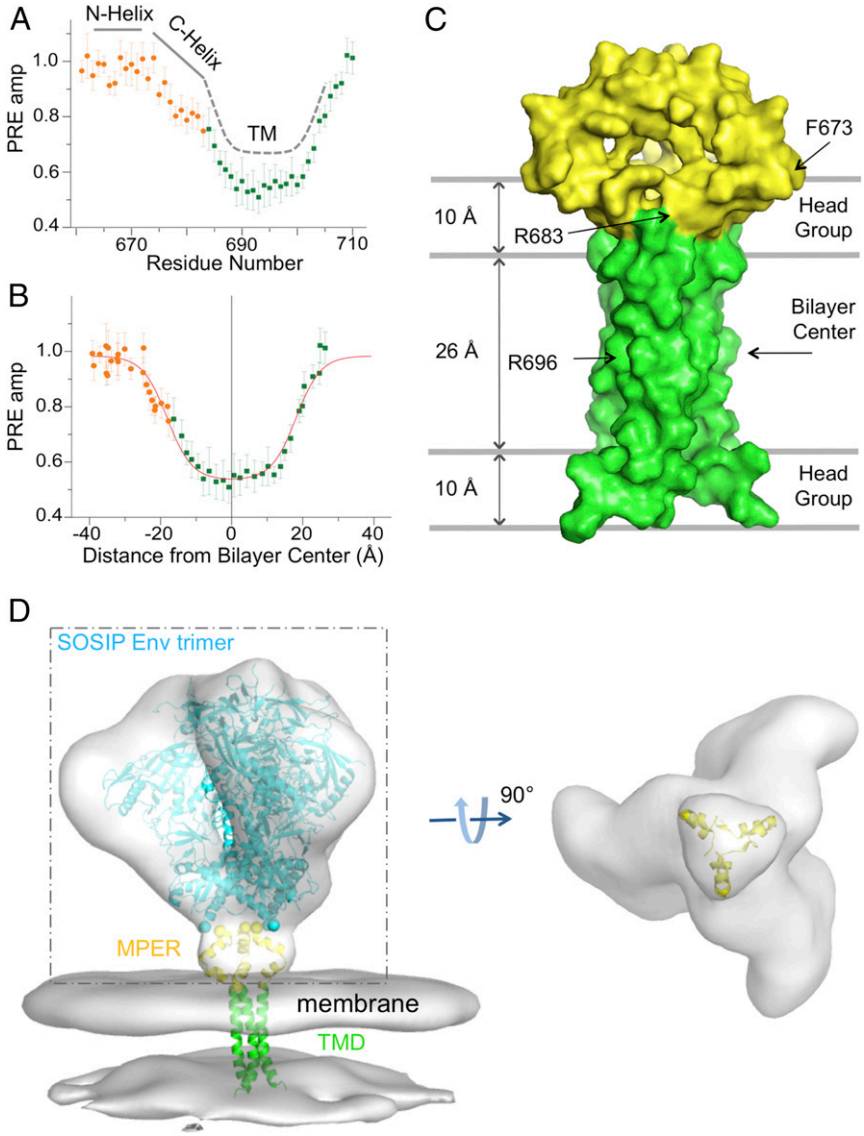

Fig. 2. Transmembrane partition of the MPER-TMD in bicelles. (*A*) Solvent PRE amplitude is plotted against residue number for the MPER-TMD with the MPER shown in orange and the TMD in green. (*B*) PRE amplitude is plotted against distance from the bilayer center along the trimer axis, fitted to the sigmoidal function. The fit is shown in red. (*C*) Position of the MPER-TMD trimer in surface representation relative to the lipid bilayer and the bilayer center with the MPER in yellow and the TMD in green. (*D*) Fit of the MPER-TMD into EM density of the HIV-1 Env trimer on the surface of virion. (*Left*) Density of the Env trimer [Electron Microscopy Data Bank (EMDB) ID: EMD-5019] and viral membrane (EMDB ID: EMD-5020), derived from cryo-ET (39), is shown in gray. The backbone trace of a natively glycosylated HIV-1 BG505 SOSIP.664 Env trimer [Protein Data Bank (PDB) ID code 5T3Z] (43), fitted to the cryo-ET density, is in light blue, the MPER in yellow, and the TMD in green. (*Right*) A view from below of the cryo-ET density within the dashed box, with the membrane density and the SOSIP backbone omitted for clarity.

slightly over 40% of the MPER-TMD binds this antibody at time 0. We conclude that the MPER-TMD in bicelles transiently samples conformations that allow antibody binding; the MPER appears to be accessible up to ∼10% of the time to the 2F5, 4E10, and 10E8 Fabs but ∼40% of time to the DH570 Fab. Constraints from the ectodomain would further restrict these fluctuations in the context of an intact Env trimer.

Roles of the MPER in Membrane Fusion. To assess possible functional roles for the MPER in membrane fusion, we generated 17 Env mutants using the sequence of a clade A isolate, 92UG037.8, guided by the new structure. We mutated each of the three structural elements: hydrophobic core, turn, and kink. When introduced into pseudoviruses, all mutants gave wild-type-like Env incorporation and processing, except the one bearing W666A in the hydrophobic core, which gave increased Env incorporation (*SI Appendix*, Fig. S7*A*). Infectivity of all mutant pseudoviruses, except the one bearing L663A near the hydrophobic core, decreased substantially (*SI Appendix*, Figs. S7 *B–D* and S8*F*). In particular, W666 in the hydrophobic core and K683 at the kink appeared to be the two most critical residues, as all of the mutants with changes at these positions lost infectivity almost completely. For the rest of the mutants, infectivity ranged from 4.3 to 50.8% of that of the wild type. Likewise, when transiently transfected in 293T cells in the absence of Gag protein, these MPER mutants expressed comparable levels of Env, with similar extents of cleavage between gp120 and gp41, as well as similar cell-surface levels (*SI Appendix*, Fig. S8 *A–C*). At a low Env expression level that mimics the low surface density on HIV-1 virions (46), most MPER mutants induced cell–cell fusion at a significantly lower level than did the

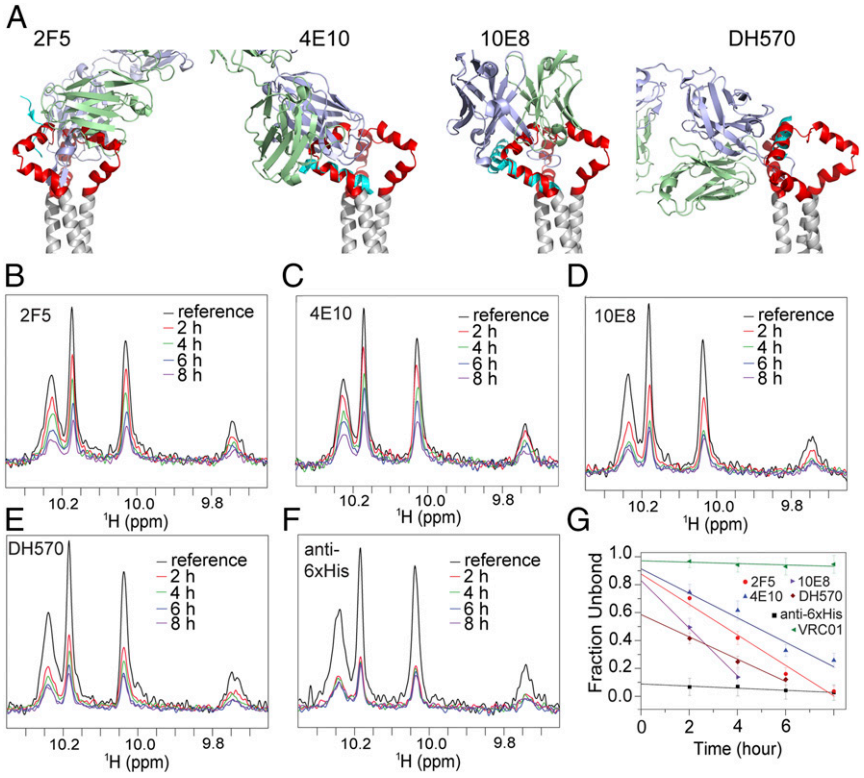

Fig. 3. Antibody accessibility of the MPER-TMD in bicelles. (*A*) The MPER-TMD structure, superposed on crystal structures of the MPER epitope peptides in the complex with their corresponding antibodies, 2F5 [PDB ID code 1TJH (20)], 4E10 [PDB ID code 2FX7 (71)], 10E8 [PDB ID code 4G6F (12)], and DH570 [PDB ID code 5DD0 (44)]. Antibody heavy and light chains are in blue and green, respectively; the epitope peptides are in cyan, the MPER trimer in red, and the TMD in gray. (*B*) Binding of the MPER-TMD to 2F5 Fab was monitored by loss of NMR signal (due to rapid signal relaxation upon Fab binding). The 1D ^{1}H-^{15}N TROSY-HSQC spectrum of the tryptophan indole amines was recorded for the MPER-TMD in bicelles ($q = 0.55$) at various time points, shown in different colors, after addition of 2F5. The reference spectrum in black was recorded without 2F5. The MPER-TMD:antibody molar ratio was 1.0:0.7. (*C*–*E*) Same as in *B* performed for the 4E10, 10E8, and DH570 Fabs, respectively. (*F*) Same as in *B* performed for the anti-6xHis Fab (prepared from antibody MA1-21315) using the MPER-TMD with an N-terminal 6xHis tag. (*G*) Fraction of Fab not bound to the MPER-TMD at various time points, calculated as $(I - 0.3)/(I_0 - 0.3)$, where I_0 is the reference peak intensity normalized to 1, I is the fraction peak intensity at a particular time relative to I_0, and subtraction of 0.3 corrected for the 30% molar excess of MPER-TMD in the mixture. The y axis intercepts indicate the fraction of the MPER-TMD in a conformation that is incompatible with antibody binding. The essentially flat line for VRC01 shows little or no binding to MPER, as expected.

wild-type Env (*SI Appendix*, Fig. S8 *D* and *F*), largely in agreement with the observations on pseudoviruses. Interactions between Env and Gag may contribute to the small discrepancies between viral infectivity and cell–cell fusion. A high Env expression level appeared to compensate for defects in membrane fusion of all less-active mutants, including those containing mutations at W666 and K683 (*SI Appendix*, Fig. S8*E*). Overall, these data indicate that the key residues important for stabilizing the MPER structure determined by NMR are also critical for Env-induced membrane fusion activity, especially in the context of viral infection.

Effect of the MPER on Antibody Sensitivity of the Env Ectodomain. We reported previously that the TMD and the cytoplasmic tail (CT) both influence the antigenic structure of the Env ectodomain (32, 47). The MPER—the only direct link connecting the TMD and CT to the ectodomain—could in principle also modulate the Env antigenic properties, and indeed increased antibody-neutralization sensitivity has been attributed to single residue changes in the MPER of certain naturally selected escape viruses (48). To determine whether or not mutations in the MPER affect epitope accessibility in other regions of the Env ectodomain, we tested several of the most active MPER mutants in a pseudovirus-based neutralization assay using bnAbs PG9, PG16, and PGT145 (trimer-specific) (49, 50) and VRC01 (CD4 binding site) (45), as well as nonneutralizing or strain-specific neutralizing antibodies, including b6 (CD4 binding site) (45), 3791 (V3) (51), and 17b (CD4-induced) (52). Pseudoviruses bearing the wild-type Env were sensitive to VRC01, PG9, PG16, and PGT145 but resistant to b6, 3791, and 17b, as expected (Fig. 4). The mutant L663A, which is near the hydrophobic core but not critical for stabilizing the observed MPER conformation, had a wild-type level of viral infectivity and an antibody sensitivity profile almost identical to that of wild-type Env. In contrast, the mutants W670A (hydrophobic core), F673A (turn), and W680A (kink), while still sensitive to VRC01, became much more resistant to the trimer-specific bnAbs and also gained sensitivity to b6, 3791, and 17b. Thus, the MPER mutations can destabilize the Env ectodomain and shift it toward an open conformation (39, 53, 54). These findings support the notion that the MPER is a control relay that modulates open and closed states of the Env trimer and exposure of other epitopes.

Discussion

We have shown that the HIV-1 gp41 MPER when connected to its TMD forms a trimeric cluster that is largely solvent-exposed on the membrane surface. The width and depth of the MPER trimer match membrane-proximal density from a low-resolution, cryo-ET–derived structure of the prefusion Env trimer on virions (Fig. 2*D*). The TMD in this construct has an NMR spectrum identical to that of the TMD alone (32). The antigenic properties of the bicelle-associated MPER-TMD are also consistent with previous studies showing that most of the known MPER-directed bnAbs recognize the prehairpin conformation of this region,

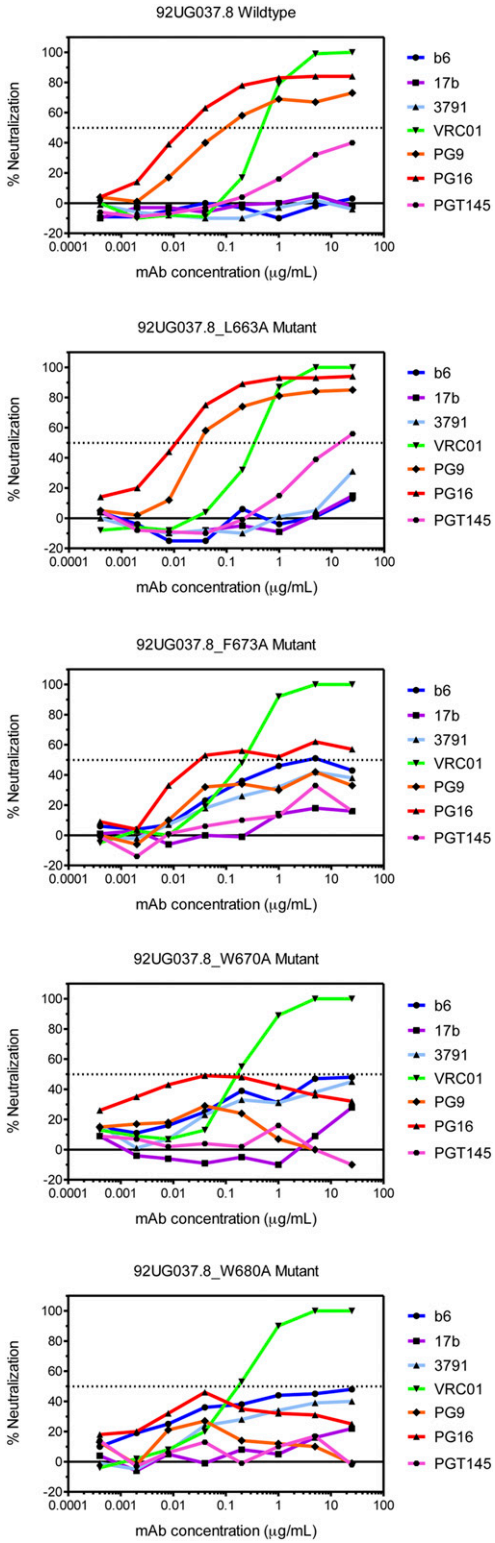

Fig. 4. Effect of mutations in the MPER on Env antibody sensitivity. Antibody neutralization of pseudoviruses containing either the wild-type 92UG037.8 Env or one of the MPER mutants shown was determined for the ordinarily nonneutralizing antibodies, b6 (CD4 binding site; blue), 3791 (V3; cyan), and 17b (CD4-induced; purple) and for the trimer-specific bnAbs, PG9 (orange), PG16 (red), and PGT145 (magenta). The CD4 binding site bnAb VRC01 (green) was a control. The experiment was performed in duplicate.

rather than its prefusion structure. From the effects on ectodomain antigenicity of mutations that destabilize the observed MPER structure, from its resemblance to the cryo-ET density, and from the likelihood that the MPER postfusion conformation will involve interaction with residues close to the fusion peptide, we propose that the conformation described here corresponds to the MPER-TMD in prefusion Env. Structures of membrane-anchored gp160 with better resolution in this region than those currently available will be needed to validate this proposal.

Prevalence of anti-MPER neutralizing antibodies in HIV-1–infected patients varies among different cohorts (12, 55–58). When present, MPER-directed neutralizing antibodies appear to correlate with greater breadth and potency of anti-HIV-1 activity (59). Early attempts to elicit 2F5- or 4E10-like antibodies primarily by MPER peptides were unsuccessful (60). Immune tolerance mechanisms have been proposed to restrict induction of these antibodies (29–31, 44, 61–63). Appreciation that phospholipids may form part of the bnAb epitopes and isolation of 10E8-like antibodies with great breadth and potency but low polyreactivity and autoreactivity have prompted renewed enthusiasm for using the MPER as a vaccine target (64, 65). Our MPER structure raises the possibility that an appropriately configured immunogen might elicit bnAbs that react with an epitope exposed on the membrane surface without accompanying polyreactivity. Indeed, a weakly neutralizing antibody (DH570) induced by vaccination in nonhuman primates shows detectable binding to the MPER in the conformation described here (Fig. 3). These results suggest that the MPER-TMD in a lipid bilayer might be a more effective immunogen than the membrane-linked peptides used in published studies. Any neutralizing antibody targeting the MPER would probably have considerable breadth, because of the high degree of sequence conservation. Whether this structure can serve as a useful vaccine template for inducing a new class of bnAbs will require further investigation.

Potent bnAbs recognize epitopes in the CD4 binding site, the V1V2-glycan region, the V3-glycan area, and the gp120–gp41 interface (66, 67). Optimal presentation of these epitopes depends on the organization of the Env trimer. We do not yet know which conformation(s) of each epitope should be presented at different stages of bnAb development, such as B cell activation and affinity maturation. Our data indicate that the MPER is critical for trimer stability and antigenicity, suggesting that we can use it as a structural modulator to alter exposure of other bnAb epitopes. The atomic details of the MPER trimer structure should enable rational protein engineering to manipulate presentation of the antigenic surfaces of Env to induce effective antibody responses.

Materials and Methods

For complete methods see *SI Appendix*.

Sample Preparation. A fragment (MPER-TMD) spanning residues 660–710 of HIV-1 gp41 (clade D, isolate 92UG024.2) was expressed in *Escherichia coli* strain BL21 (DE3) cells as a trpLE fusion and isolated by Ni-NTA affinity purification, cyanogen bromide cleavage, and reverse-phase HPLC as previously described (32). Pure MPER-TMD was reconstituted in DMPC/DHPC bicelles with [DMPC]/[DHPC] (q) between 0.5 and 0.6. A typical NMR sample contained ~0.8 mM MPER-TMD (monomer), ~50 mM DMPC, ~100 mM DHPC, 40 mM MOPS (pH 6.7), 0.02% NaN_3, and 5% D_2O. For perdeuterated proteins, cells were adapted in 100 mL M9 minimal media (~97% D_2O) and then grown at large scale (4 L) in 99.8% D_2O with deuterated glucose. For NOE experiments, the protein was reconstituted using DMPC and DHPC with perdeuterated acyl chains.

Oligomeric State. The bicelle-reconstituted MPER-TMD was mixed with a SDS sample buffer without boiling, followed by SDS/PAGE (*SI Appendix*, Fig. S1*C*). The MPER-TMD protein migrated at ~17 kDa, the size of a trimer (~18.5 kDa). We confirmed this interpretation by chemical cross-linking and urea-PAGE (*SI Appendix*, Fig. S1*D*). We made the double mutant K665R/D674K, designed retrospectively based on the MPER-TMD structure, to facilitate cross-linking with dithiobis-succinimidyl propionate.

NMR Resonance Assignment. All NMR data were collected at 35 °C. Sequence-specific assignment of backbone chemical shifts used transverse relaxation optimized spectroscopy (TROSY)-enhanced triple resonance experiments (68), confirmed with a 3D ^{15}N-edited NOESY-TROSY-HSQC (heteronuclear single-quantum correlation) spectrum. Protein sidechain resonances were assigned by a combination of 3D ^{15}N-edited NOESY-TROSY and ^{13}C-edited NOESY-HSQC spectra, recorded using a (^{15}N, ^{13}C)-labeled protein sample in deuterated bicelles. For residues 685–702, the methyl group assignments were taken from those of the TMD in our previous study, as their chemical shifts were essentially identical.

NMR Structure Determination. We used the following general approach: (*i*) determine local structure of an individual chain in the oligomer, (*ii*) apply intermonomer distance restraints to derive the oligomer structure, (*iii*) cross-validate the NOE-derived structure using PRE from spin labels, and (*iv*) determine the transmembrane partition in bicelles by PPT (38). We determined secondary structures of the subunits in the oligomeric complex using local NOE restraints and backbone dihedral restraints derived from chemical shifts and TALOS+ (69). We then identified intermonomer contacts using a mixed sample with differentially labeled monomers to record NOEs between the ^{15}N-attached protons of one monomer and nonexchangeable protons of the neighboring monomers. We used a negative control sample to confirm the intermonomer NOEs. The MPER-TMD trimer structure was calculated using X-PLOR-NIH (70) and refined against all dihedral and NOE restraints. As independent validation, we performed PRE analysis on a mixed sample containing ~1:1 ratio of (^{15}N, ~70% ^{2}H)-labeled MPER-TMD and ^{14}N MPER-TMD tagged with MTSL at position 660 or 710. We determined the transmembrane partition of the MPER-TMD trimer in bicelles by PPT (38).

Fab Binding to the MPER-TMD in Bicelles. We tested Fab binding to (^{15}N, 80% ^{2}H)-labeled MPER-TMD in bicelles (q = 0.5); association with Fab will completely attenuate NMR signals in 1D, ^{15}N-edited TROSY-HSQC spectra from the MPER-TMD. For binding to 2F5 or 4E10 Fab, we used the wild-type MPER-TMD. For binding to the anti-His Fab, we used the MPER-TMD with N-terminal 6His-tag.

ACKNOWLEDGMENTS. We thank J. Chen for technical assistance, D. Barouch and B. Haynes for critical reading of the manuscript, and the NIH AIDS Reagent Program, Division of AIDS, National Institute of Allergy and Infectious Diseases for reagents. This work was supported by NIH Grants AI127193 (to B.C. and J.J.C.), AI106488 (to B.C.), and AI129721 (to B.C.), the Center for HIV/AIDS Vaccine Immunology–Immunogen Design Grant AI-100645 (to S.C.H.), a Merck Fellowship (Q.F.), and Collaboration for AIDS Vaccine Discovery Grant OPP1169339 (to B.C. from the Bill and Melinda Gates Foundation). The NMR data were collected at the NMR facility of National Center for Protein Science Shanghai (supported by Chinese Academy of Sciences Grant XDB08030301) and MIT-Harvard CMR (supported by NIH Grant P41 EB-002026). S.C.H. is an Investigator in the Howard Hughes Medical Institute.

1. Wei X, et al. (2003) Antibody neutralization and escape by HIV-1. *Nature* 422:307–312.
2. Richman DD, Wrin T, Little SJ, Petropoulos CJ (2003) Rapid evolution of the neutralizing antibody response to HIV type 1 infection. *Proc Natl Acad Sci USA* 100:4144–4149.
3. Harrison SC (2005) Mechanism of membrane fusion by viral envelope proteins. *Adv Virus Res* 64:231–261.
4. Chan DC, Kim PS (1998) HIV entry and its inhibition. *Cell* 93:681–684.
5. Weissenhorn W, Dessen A, Harrison SC, Skehel JJ, Wiley DC (1997) Atomic structure of the ectodomain from HIV-1 gp41. *Nature* 387:426–430.
6. Chan DC, Fass D, Berger JM, Kim PS (1997) Core structure of gp41 from the HIV envelope glycoprotein. *Cell* 89:263–273.
7. Dimitrov AS, Rawat SS, Jiang S, Blumenthal R (2003) Role of the fusion peptide and membrane-proximal domain in HIV-1 envelope glycoprotein-mediated membrane fusion. *Biochemistry* 42:14150–14158.
8. Muñoz-Barroso I, Salzwedel K, Hunter E, Blumenthal R (1999) Role of the membrane-proximal domain in the initial stages of human immunodeficiency virus type 1 envelope glycoprotein-mediated membrane fusion. *J Virol* 73:6089–6092.
9. Salzwedel K, West JT, Hunter E (1999) A conserved tryptophan-rich motif in the membrane-proximal region of the human immunodeficiency virus type 1 gp41 ectodomain is important for Env-mediated fusion and virus infectivity. *J Virol* 73:2469–2480.
10. Muster T, et al. (1993) A conserved neutralizing epitope on gp41 of human immunodeficiency virus type 1. *J Virol* 67:6642–6647.
11. Stiegler G, et al. (2001) A potent cross-clade neutralizing human monoclonal antibody against a novel epitope on gp41 of human immunodeficiency virus type 1. *AIDS Res Hum Retroviruses* 17:1757–1765.
12. Huang J, et al. (2012) Broad and potent neutralization of HIV-1 by a gp41-specific human antibody. *Nature* 491:406–412.
13. Williams LD, et al. (2017) Potent and broad HIV-neutralizing antibodies in memory B cells and plasma. *Sci Immunol* 2:eaal2200.
14. Sun ZY, et al. (2008) HIV-1 broadly neutralizing antibody extracts its epitope from a kinked gp41 ectodomain region on the viral membrane. *Immunity* 28:52–63.
15. Kim M, et al. (2011) Antibody mechanics on a membrane-bound HIV segment essential for GP41-targeted viral neutralization. *Nat Struct Mol Biol* 18:1235–1243.
16. Liu J, Deng Y, Dey AK, Moore JP, Lu M (2009) Structure of the HIV-1 gp41 membrane-proximal ectodomain region in a putative prefusion conformation. *Biochemistry* 48: 2915–2923.
17. Buzon V, et al. (2010) Crystal structure of HIV-1 gp41 including both fusion peptide and membrane proximal external regions. *PLoS Pathog* 6:e1000880.
18. Shi W, et al. (2010) Structural characterization of HIV gp41 with the membrane-proximal external region. *J Biol Chem* 285:24290–24298.
19. Lee JH, Ozorowski G, Ward AB (2016) Cryo-EM structure of a native, fully glycosylated, cleaved HIV-1 envelope trimer. *Science* 351:1043–1048.
20. Ofek G, et al. (2004) Structure and mechanistic analysis of the anti-human immunodeficiency virus type 1 antibody 2F5 in complex with its gp41 epitope. *J Virol* 78: 10724–10737.
21. Pejchal R, et al. (2009) A conformational switch in human immunodeficiency virus gp41 revealed by the structures of overlapping epitopes recognized by neutralizing antibodies. *J Virol* 83:8451–8462.
22. Irimia A, Sarkar A, Stanfield RL, Wilson IA (2016) Crystallographic identification of lipid as an integral component of the epitope of HIV broadly neutralizing antibody 4E10. *Immunity* 44:21–31.
23. Irimia A, et al. (2017) Lipid interactions and angle of approach to the HIV-1 viral membrane of broadly neutralizing antibody 10E8: Insights for vaccine and therapeutic design. *PLoS Pathog* 13:e1006212.
24. Alam SM, et al. (2009) Role of HIV membrane in neutralization by two broadly neutralizing antibodies. *Proc Natl Acad Sci USA* 106:20234–20239.
25. Scherer EM, Leaman DP, Zwick MB, McMichael AJ, Burton DR (2010) Aromatic residues at the edge of the antibody combining site facilitate viral glycoprotein recognition through membrane interactions. *Proc Natl Acad Sci USA* 107:1529–1534.
26. Song L, et al. (2009) Broadly neutralizing anti-HIV-1 antibodies disrupt a hinge-related function of gp41 at the membrane interface. *Proc Natl Acad Sci USA* 106:9057–9062.
27. Frey G, et al. (2008) A fusion-intermediate state of HIV-1 gp41 targeted by broadly neutralizing antibodies. *Proc Natl Acad Sci USA* 105:3739–3744.
28. Chen J, et al. (2014) Mechanism of HIV-1 neutralization by antibodies targeting a membrane-proximal region of gp41. *J Virol* 88:1249–1258.
29. Haynes BF, et al. (2005) Cardiolipin polyspecific autoreactivity in two broadly neutralizing HIV-1 antibodies. *Science* 308:1906–1908.
30. Yang G, et al. (2013) Identification of autoantigens recognized by the 2F5 and 4E10 broadly neutralizing HIV-1 antibodies. *J Exp Med* 210:241–256.
31. Liu M, et al. (2015) Polyreactivity and autoreactivity among HIV-1 antibodies. *J Virol* 89:784–798.
32. Dev J, et al. (2016) Structural basis for membrane anchoring of HIV-1 envelope spike. *Science* 353:172–175.
33. Rowell JF, Stanhope PE, Siliciano RF (1995) Endocytosis of endogenously synthesized HIV-1 envelope protein. Mechanism and role in processing for association with class II MHC. *J Immunol* 155:473–488.
34. Boge M, Wyss S, Bonifacino JS, Thali M (1998) A membrane-proximal tyrosine-based signal mediates internalization of the HIV-1 envelope glycoprotein via interaction with the AP-2 clathrin adaptor. *J Biol Chem* 273:15773–15778.
35. Fu Q, et al. (2016) Structural basis and functional role of intramembrane trimerization of the Fas/CD95 death receptor. *Mol Cell* 61:602–613.
36. Chiliveri SC, Louis JM, Ghirlando R, Baber JL, Bax A (2018) Tilted, uninterrupted, monomeric HIV-1 gp41 transmembrane helix from residual dipolar couplings. *J Am Chem Soc* 140:34–37.
37. Shen X, et al. (2010) Prolonged exposure of the HIV-1 gp41 membrane proximal region with L669S substitution. *Proc Natl Acad Sci USA* 107:5972–5977.
38. Piai A, Fu Q, Dev J, Chou JJ (2017) Optimal bicelle size q for solution NMR studies of the protein transmembrane partition. *Chemistry* 23:1361–1367.
39. Liu J, Bartesaghi A, Borgnia MJ, Sapiro G, Subramaniam S (2008) Molecular architecture of native HIV-1 gp120 trimers. *Nature* 455:109–113.
40. Julien JP, et al. (2013) Crystal structure of a soluble cleaved HIV-1 envelope trimer. *Science* 342:1477–1483.
41. Lyumkis D, et al. (2013) Cryo-EM structure of a fully glycosylated soluble cleaved HIV-1 envelope trimer. *Science* 342:1484–1490.
42. Pancera M, et al. (2014) Structure and immune recognition of trimeric pre-fusion HIV-1 Env. *Nature* 514:455–461.
43. Gristick HB, et al. (2016) Natively glycosylated HIV-1 Env structure reveals new mode for antibody recognition of the CD4-binding site. *Nat Struct Mol Biol* 23:906–915.
44. Zhang R, et al. (2016) Initiation of immune tolerance-controlled HIV gp41 neutralizing B cell lineages. *Sci Transl Med* 8:336ra62.
45. Scheid JF, et al. (2011) Sequence and structural convergence of broad and potent HIV antibodies that mimic CD4 binding. *Science* 333:1633–1637.
46. Zhu P, et al. (2006) Distribution and three-dimensional structure of AIDS virus envelope spikes. *Nature* 441:847–852.
47. Chen J, et al. (2015) HIV-1 ENVELOPE. Effect of the cytoplasmic domain on antigenic characteristics of HIV-1 envelope glycoprotein. *Science* 349:191–195.
48. Bradley T, et al. (2016) Amino acid changes in the HIV-1 gp41 membrane proximal region control virus neutralization sensitivity. *EBioMedicine* 12:196–207.
49. Walker LM, et al.; Protocol G Principal Investigators (2009) Broad and potent neutralizing antibodies from an African donor reveal a new HIV-1 vaccine target. *Science* 326:285–289.

50. Walker LM, et al.; Protocol G Principal Investigators (2011) Broad neutralization coverage of HIV by multiple highly potent antibodies. *Nature* 477:466–470.
51. Swetnam J, Shmelkov E, Zolla-Pazner S, Cardozo T (2010) Comparative magnitude of cross-strain conservation of HIV variable loop neutralization epitopes. *PLoS One* 5: e15994.
52. Thali M, et al. (1993) Characterization of conserved human immunodeficiency virus type 1 gp120 neutralization epitopes exposed upon gp120-CD4 binding. *J Virol* 67: 3978–3988.
53. Wang H, et al. (2016) Cryo-EM structure of a CD4-bound open HIV-1 envelope trimer reveals structural rearrangements of the gp120 V1V2 loop. *Proc Natl Acad Sci USA* 113:E7151–E7158.
54. Ozorowski G, et al. (2017) Open and closed structures reveal allostery and pliability in the HIV-1 envelope spike. *Nature* 547:360–363.
55. Morris L, et al. (2011) Isolation of a human anti-HIV gp41 membrane proximal region neutralizing antibody by antigen-specific single B cell sorting. *PLoS One* 6:e23532.
56. Molinos-Albert LM, et al. (2014) Anti-MPER antibodies with heterogeneous neutralization capacity are detectable in most untreated HIV-1 infected individuals. *Retrovirology* 11:44.
57. Pietzsch J, et al. (2010) Anti-gp41 antibodies cloned from HIV-infected patients with broadly neutralizing serologic activity. *J Virol* 84:5032–5042.
58. Landais E, et al. (2016) Broadly neutralizing antibody responses in a large longitudinal Sub-Saharan HIV primary infection cohort. *PLoS Pathog* 12:e1005369.
59. Jacob RA, et al. (2015) Anti-V3/glycan and anti-MPER neutralizing antibodies, but not anti-V2/glycan site antibodies, are strongly associated with greater anti-HIV-1 neutralization breadth and potency. *J Virol* 89:5264–5275.
60. Montero M, van Houten NE, Wang X, Scott JK (2008) The membrane-proximal external region of the human immunodeficiency virus type 1 envelope: Dominant site of antibody neutralization and target for vaccine design. *Microbiol Mol Biol Rev* 72: 54–84.
61. Verkoczy L, et al. (2010) Autoreactivity in an HIV-1 broadly reactive neutralizing antibody variable region heavy chain induces immunologic tolerance. *Proc Natl Acad Sci USA* 107:181–186.
62. Chen Y, et al. (2013) Common tolerance mechanisms, but distinct cross-reactivities associated with gp41 and lipids, limit production of HIV-1 broad neutralizing antibodies 2F5 and 4E10. *J Immunol* 191:1260–1275.
63. Verkoczy L, et al. (2013) Induction of HIV-1 broad neutralizing antibodies in 2F5 knock-in mice: Selection against membrane proximal external region-associated autoreactivity limits T-dependent responses. *J Immunol* 191:2538–2550.
64. Donius LR, et al. (2016) Generation of long-lived bone marrow plasma cells secreting antibodies specific for the HIV-1 gp41 membrane-proximal external region in the absence of polyreactivity. *J Virol* 90:8875–8890.
65. Lutje Hulsik D, et al. (2013) A gp41 MPER-specific llama VHH requires a hydrophobic CDR3 for neutralization but not for antigen recognition. *PLoS Pathog* 9:e1003202.
66. Kwong PD, Mascola JR, Nabel GJ (2013) Broadly neutralizing antibodies and the search for an HIV-1 vaccine: The end of the beginning. *Nat Rev Immunol* 13:693–701.
67. Klein F, et al. (2013) Antibodies in HIV-1 vaccine development and therapy. *Science* 341:1199–1204.
68. Salzmann M, Wider G, Pervushin K, Wüthrich K (1999) Improved sensitivity and coherence selection for [15N,1H]-TROSY elements in triple resonance experiments. *J Biomol NMR* 15:181–184.
69. Shen Y, Delaglio F, Cornilescu G, Bax A (2009) TALOS+: A hybrid method for predicting protein backbone torsion angles from NMR chemical shifts. *J Biomol NMR* 44: 213–223.
70. Schwieters CD, Kuszewski JJ, Tjandra N, Clore GM (2003) The Xplor-NIH NMR molecular structure determination package. *J Magn Reson* 160:65–73.
71. Cardoso RM, et al. (2007) Structural basis of enhanced binding of extended and helically constrained peptide epitopes of the broadly neutralizing HIV-1 antibody 4E10. *J Mol Biol* 365:1533–1544.

PNAS
www.pnas.org

Supplementary Information for

Structure of the membrane proximal external region of HIV-1 envelope glycoprotein

James J. Chou,
email: james_chou@hms.harvard.edu;
Bing Chen,
email: bchen@crystal.harvard.edu;
Stephen C. Harrison,
email: harrison@crystal.harvard.edu

This PDF file includes:

www.pnas.org/cgi/doi/10.1073/pnas.1807529115

SI Methods

Protein expression and purification

Addition of the MPER to our previous gp41$^{HIV1D(677-716)}$ construct led to severe protein aggregation. We therefore tested several HIV-1 gp41 fragments, including 660-716, 660-710, 665-716, 671-716, and 660-705, and found that the 660-710 fragment from HIV-1 clade D isolate 92UG024.2 was very stable in DMPC/DHPC bicelles with $0.5 \leq q \leq 0.6$, showing excellent solution NMR properties. This construct, designated gp41$^{HIV1D(660-710)}$ or MPER-TMD, contains the entire MPER (residues 660-683) and the TMD (residues 684-705). The expression construct of the MPER-TMD was created as a trpLE fusion following a procedure described previously (1). Mutant constructs were generated by standard PCR protocols and confirmed by DNA sequencing. For NMR sample preparation, transformed *E. coli* strain BL21 (DE3) cells were grown in M9 minimal media supplemented with Centrum multivitamins and stable isotopes. Cultures were grown at 37° C to an absorbance of ~0.6 at 600 nm, and cooled to 22° C before induction with 100 μM isopropyl β-D-thiogalatopyranoside at 22° C for overnight. For fully deuterated proteins, bacterial culture in 1 ml LB medium was spun down and the cells were adapted in 99.8% D_2O medium (100 ml, with deuterated glucose) over night. Then collected cells were grown in 99.8% D_2O (4 L) (Sigma Aldrich, St. Louis, MO) with deuterated glucose (Cambridge Isotope Laboratories, Tewksbury, MA). The MPER-TMD protein was extracted, cleaved by cyanogen bromide, purified and lyophilized as described (1). Protein identity was confirmed by MALDI-TOF mass spectrometry and SDS-PAGE.

Reconstitution of the MPER-TMD in bicelles

To reconstitute the MPER-TMD in bicelles, 2 mg of lyophilized protein was mixed with 9 mg 1,2-dimyristoyl-*sn*-Glycero-3-Phosphocholine (DMPC; protonated or deuterated from Avanti Ploar Lipids, Alabaster, AL) and dissolved in hexafluoro-isopropanal. The mixture was slowly dried to a thin film under nitrogen stream, followed by overnight lyophilization. The dried thin film was redissolved in 3 ml of 8 M urea containing ~20 mg 1,2-dihexanoyl-*sn*-Glycero-3-Phosphocholine (D6PC; protonated or deuterated from Avanti Polar Lipids), with subsequent addition of ~2-4 mg 1,2-diheptanoyl-*sn*-Glycero-3-Phosphocholine (D7PC; protonated or deuterated from Avanti Polar Lipids). D7PC, with a critical micelle concentration (CMC) of ~1.4 mM, was used to prevent formation of liposomes, because D6PC, which has a CMC of ~ 15 mM, is often lost very rapidly during dialysis. The mixture was dialyzed twice against a 40 mM MOPS buffer (pH 6.8) (1 L each time) to remove the denaturant, and 15 mg D6PC was added to the sample before the second dialysis to compensate its loss. After the

second dialysis, we estimate that D7PC accounted for less than 5% of the total detergent (D6PC and D7PC). The DMPC:DHPC ratio was monitored by 1D NMR throughout the reconstitution process. If needed, additional D6PC was added to make the final DMPC: DHPC ratio between 0.5 and 0.6. The sample was concentrated in a Centricon (EMD Millipore, Billerica, MA) to ~350 μl. The final NMR sample contained ~0.8 mM MPER-TMD (monomer), ~50 mM DMPC, ~100 mM D6PC, 40 mM MOPS (pH 6.7), 0.02% NaN_3 and 5% D_2O. For all NOE experiments, the protein was reconstituted using DMPC and DHPC with deuterated acyl chains (Avanti Polar Lipids).

Analysis of the oligomeric state of the MPER-TMD in bicelles by SDS-PAGE and chemical crosslinking

Wild type MPER-TMD was reconstituted in bicelles (q=0.5), then mixed with a SDS sample buffer (Invitrogen) without boiling, followed by SDS-PAGE at 200 volts for 30 minutes and Commassie blue staining. The MPER-TMD protein migrated slightly faster that than did a marker protein with M.W. of 18 kDa (Fig. S1B), consistent with the theoretical size of a trimer (~18.5 kDa).

As an independent validation, we examined trimerization of the MPER-TMD in bicelles (q=0.5) by chemical crosslinking followed by urea-PAGE. Double mutation K665R/D674K was introduced retrospectively using the structure of the MPER-TMD to facilitate crosslinking with dithiobis-succinimidyl propionate (DSP). DSP was dissolved in DMSO at 200 mM, and added to reconstituted MPER-TMD (K665R/D674K) at 0.05 mM (monomer) concentration. Cross-linking was performed using DSP at a final concentration of 0.6 mM for 30 min at room temperature, and the reaction was quenched with 200 mM Tris buffer (pH 7.5) and then used for UREA-PAGE. The mutant MPER-TMD migrated in 8 M urea as a diffuse band at roughly the position expected for a monomer; the DSP-treated mutant migrated predominantly as a sharp band at the position expected for a trimer (M.W. ~20 kDa including DSP) (Fig. S1D).

NMR spectroscopy

Assignment of NMR resonances. All NMR data were collected at 35°C on Bruker spectrometers operating at ^1H frequency of 900 MHz, 800 MHz, 750 MHz, or 600 MHz and equipped with cryogenic probes. NMR data were processed using NMRPipe (2), and spectra were analyzed using NMRPipe (2), Sparky (T. D. Goddard and D. G. Kneller, SPARKY 3, University of California, San Francisco), and XEASY (3). Sequence specific assignment of backbone chemical shifts was accomplished using two pairs of TROSY-enhanced triple resonance experiments (4), recorded from a (^{15}N, ^{13}C, 85% ^2H)-

labeled sample. The triple resonance experiments included HNCA, HN(CO)CA, HN(CA)CO, and HNCO. Backbone amide resonance assignments were confirmed with a 3D ^{15}N-edited NOESY-TROSY-HSQC spectrum (τ_{NOE} = 200 ms), which was recorded on a 750 MHz spectrometer from a (^{15}N, ^{2}H)-labeled sample. Protein aliphatic and aromatic resonances were assigned using a combination of 2D ^{13}C HSQC, 3D ^{15}N-edited NOESY-TROSY (τ_{NOE} = 120 ms) and ^{13}C-edited NOESY-HSQC (τ_{NOE} = 150 ms) recorded on a 900 MHz spectrometer. These experiments were performed with (^{15}N, ^{13}C)-labeled protein samples in bicelles with deuterated DMPC and DHPC acyl chains (Anatrace). For residues 685-702, most assignments of methyl group resonances were taken directly from those of our previous TMD structure (BMRB accession number 30090), as chemical shifts for those residues are essentially the same for the MPER-TMD and TMD. Specific stereo assignment of the methyl groups of valines and leucines were obtained from a 28 ms constant-time ^{1}H-^{13}C HSQC spectrum recorded using a 15% ^{13}C-labeled sample (5). Finally, the assignment of the indole amine of W672 and W680 was confirmed using a W672Y mutant.

Backbone chemical shift and TALOS+ analyses. The assigned chemical shift values of backbone ^{15}N, ^{13}Cα, and ^{13}C' were used as input for the TALOS+ program (6) to predict backbone dihedral angles. Out of 48 residues with assignments, the dihedral angles of 42 residues were considered by TALOS+ as 'GOOD'. Furthermore, the carbon secondary shifts of gp41$^{HIV1D(660-710)}$ and gp41$^{HIV1D(677-716)}$ are compared in Fig. S2D&E, which provided a secondary structure mapping of residues 660-716 of HIV-1 Env.

Assignment of NOE restraints. Intramolecular distance restraints derived from nuclear Overhauser enhancements (NOEs) were obtained from the ^{15}N-edited and ^{13}C-edited NOESY spectra recorded on a 900 MHz spectrometer (see above). Many backbone amide resonances between 682 and 701 were extremely weak in non-deuterated protein. Thus, in the ^{15}N-edited NOESY recorded with the non-deuterated protein, most of the local NOEs could not be analyzed. The spectrum of residues 685-702 is, however, the same as that of the gp41$^{HIV1D(677-716)}$ sample (Fig. S2A&B). We thus applied the NOE restraints assigned for residues 685-702 of the gp41$^{HIV1D(677-716)}$ sample.

Determining the inter-protomer distance restraints faced the challenge of measuring NOEs between structurally equivalent protomers having the same chemical shifts. To solve this problem, we prepared a mixed sample in which half of the protomers were ^{15}N, ^{2}H-labeled (0.4 mM) and the other half 15% ^{13}C-labeled (0.4 mM). Recording a 3D ^{15}N-edited NOESY-TROSY-HSQC (τ_{NOE} = 200 ms)

on this sample allowed measurement of exclusive NOEs between the ^{15}N-attached protons of one subunit and aliphatic protons of the neighboring subunits. The non-deuterated peptide was 15% ^{13}C-labeled for recording the ^{1}H-^{13}C HSQC spectrum as an internal aliphatic proton chemical shift reference. Examples of residues in the MPER that had inter-protomer NOEs are shown in Fig. S3A&B. In parallel, a control sample with only (^{15}N, ^{2}H)-labeled MPER-TMD (0.4 mM) was used to record an identical 3D ^{15}N-edited NOESY-TROSY-HSQC (Fig. S3A&B). The ^{15}N, ^{2}H-labeled MPER-TMD in the mixed and control samples were from the same protein expression batch. Comparison of the mixed and control spectra allowed rigorous confirmation that a particular inter-protomer NOE was due solely to the mixing of protomers with different labeling schemes.

Structure calculation

Structures were calculated with XPLOR-NIH (7). The matching resonances, shown in Fig. S2, between gp41$^{HIV1D(660-710)}$ and gp41$^{HIV1D(677-716)}$ for the TM core (residues 685-702) justified the strategy to determine the MPER structure using the known structure of the TM core as a starting point (1). To implement this strategy, we first modeled secondary structures of the MPER-TMD monomer using the 'GOOD' dihedral angles generated by TALOS+ using backbone chemical shift values (6). Second, a trimer was assembled using the previously assigned NOE restraints for residues 685-702 (taken from PDB accession code: 5JYN). Finally, we applied the newly assigned inter-protomer restraints (most of them from residues 660-683) to complete the trimer of the MPER-TMD. For each inter-protomer restraint between two adjacent protomers, three identical distance restraints were assigned respectively to all pairs of neighboring protomers to satisfy the condition of C3 symmetry. The assembled trimer was then refined against the complete set of NOE restraints (both intra-protomer and inter-protomer) and dihedral angles using a simulated annealing (SA) protocol in which the temperature was lowered from 1000 to 200 K in steps of 40 K. The NOE restraints were enforced by flat-well harmonic potentials, with the force constant ramped from 2 to 50 kcal/mol Å^{-2} during annealing. Backbone dihedral angle restraints were taken from the 'GOOD' dihedral angles from TALOS+, all with a flat-well (± the corresponding uncertainties from TALOS+) harmonic potential with force constant ramped from 10 to 1000 kcal/mol rad^{-2}. A total of 150 structures were calculated, and the 15 lowest energy structures were selected as the final structural ensemble (Fig. S4C and Table S1).

Can we account for the observations in Chiliveri et al (8), who concluded that a construct essentially identical to the one that yielded our previous TMD structure was monomeric rather than trimeric? Their spectra were recorded at 45°C rather than 35°, a possible distinction. We believe,

however, that their data are also consistent with a stable trimer, as indeed suggested by the SDS gel in the supplementary material of that paper. Two sets of NMR observations were presented as showing lack of oligomer. With regard to the alignment tensor derived from residual dipolar coupling measurements they performed, those authors state that for a "C3 symmetric structure, alignment in an anisotropic medium must be axially symmetric, with the unique axis of the alignment tensor coinciding with the C3 axis." This will not be the case, however, if there are non-C3-symmetric fluctuations in the trimer. The C-terminal part of the TMD (the "hydrophilic core") indeed shows substantial dynamics, and there is no a priori reason to suppose that those fluctuations will be symmetrical. They also write that they were unable to detect cross-chain PRE. We have found that unless the two chains (in this case, the spin-labeled chain and the ^{15}N-labeled chain) are mixed in the trpLE-fusion form *before* purification, the trimers that form after CNBr cleavage and subsequent isolation are too stable to exchange. According to the Chiliveri et al paper (8), the chains in their experiments were mixed after purification, and we believe that they may have had a mixture of homotrimers.

^{13}C selective inter-protomer NOE experiment

For definitive assignment of inter-molecular NOE cross peaks, we prepared an isotopically mixed sample in which half of the proteins were (^{15}N, ^{2}H) labeled and the other half (^{13}C, ^{1}H) labeled. The new NOE experiment was based on the same 3D ^{15}N-edited NOESY-TROSY-HSQC as above, but used the ^{1}H-^{13}C J coupling to distinguish inter vs. intra -molecular NOEs. The ^{1}H evolution (or frequency labeling) period before the NOE mixing was changed to a “mixed constant-time” evolution to introduce ^{1}H-^{13}C J evolutions. Two interleaved 3D spectra were recorded. In one case, the total J evolution was 0 ms, making both inter and intra -molecular NOE peaks positive. In the other case, the total J evolution was 8 ms, making intermolecular NOE peaks negative and intra-molecular NOE peaks positive. Collecting the two data sets interleaved with each other allowed us to add the two spectra to see only intra-molecular NOEs or to subtract the two spectra to see only inter-molecular NOEs.

Measurement of inter-protomer PRE

To obtain inter-protomer information independent of NOEs, we performed PRE analysis on a mixed sample containing ~1:1 ratio of (^{15}N, ~70% ^{2}H) labeled MPER-TMD and ^{14}N MPER-TMD with a Cys mutation at position 660 or 710, reconstituted in bicelles with q = 0.5. Cells that expressed the two proteins with different labeling schemes were mixed prior to purification. After bicelle reconstitution, 100 mM MTSL dissolved in DMSO was added to the samples at a final ratio (MTSL to MPER-TMD)

of 5:1 and the mixture incubated at room temperature overnight. The sample was then passed through a PD-10 desalting column to remove free MTSL. DHPC was added to the final sample to adjust the q to ~0.5. For measuring PRE, defined as the ratio of peak intensities of the non-reduced (I) and reduced (I_0) samples, the ^{1}H-^{15}N TROSY-HSQC spectrum was recorded before and after the addition of 10 mM sodium ascorbate. A mixed TMD sample, labeled at position 716, was prepared similarly.

Solvent PRE analysis of TM partition

We use a previously published solvent PRE method (9) to determine the transmembrane partition of the MPER-TMD trimer in bicelles. This method is based on the notion that if the bicelle is sufficiently wide (q > 0.5), the lateral solvent PRE becomes negligible, thus allowing the use of measurable solvent PRE to probe residue-specific depth immersion of the protein in the bilayer region of the bicelle (Fig. S6). To ensure that our bicelles are wide enough, we reconstituted the MPER-TMD in bicelles with q = 0.6 (Fig. S6A) to perform the solvent PRE analysis as described in ref (9). The water-soluble and membrane-inaccessible paramagnetic agent, Gd-DOTA (Sigma), was used to generate solvent PREs. Gd-DOTA (in 200 mM stock solution) was titrated into the bicelle sample to reach final concentrations of 0.0, 1.0, 2.0, 4.0, 6.0, 8.0, 10.0 and 15.0 mM. At each concentration, a 2D ^{1}H-^{15}N TROSY-HSQC spectrum was recorded at 600 MHz to measure residue-specific PRE, defined here as the ratio of peak intensity in the presence (I) and absence (I_0) of the paramagnetic agent. Peak intensities were measured at peak local maxima using quadratic interpolation to identify peak centers. For each of the residues, we used *Origin* (OriginLab, Northampton, MA) to fit the PRE titration curve to exponential decay

$$\frac{I}{I_0} = 1 - \mathrm{PRE}_{\mathrm{amp}}\left(1 - \ e^{-[\text{Gd-DOTA}]/\tau}\right) \qquad (1)$$

to derive the residue-specific PRE amplitude ($\mathrm{PRE}_{\mathrm{amp}}$) (Fig. S6B). To determine the position of the MPER-TMD trimer relative to the bilayer center, we calculated, for each residue i, the distance (r_z) along the protein symmetry axis, which is parallel to the bilayer normal, from the amide proton to an arbitrary reference point based on the structure of the MPER-TMD trimer. This calculation converted $\mathrm{PRE}_{\mathrm{amp}}$ vs. (residue number) to $\mathrm{PRE}_{\mathrm{amp}}$ vs. r_z, which was then analyzed using *the sigmoidal fitting* method (see detailed discussion in ref (9)). Briefly, the trimer structure was moved along the 3-fold axis in increment of 0.3 Å (Fig. S6C) to achieve the best fit to the symmetric sigmoid equation

$$\mathrm{PRE}_{\mathrm{amp}} = \mathrm{PRE}_{\mathrm{amp}}^{\mathrm{min}} + \frac{\left(\mathrm{PRE}_{\mathrm{amp}}^{\mathrm{max}} - \mathrm{PRE}_{\mathrm{amp}}^{\mathrm{min}}\right)}{1+e^{\left(r_Z^I - |r_Z|\right)/\mathrm{SLOPE}}}\ , \qquad (2)$$

where $\mathrm{PRE}_{\mathrm{amp}}^{\mathrm{min}}$ and $\mathrm{PRE}_{\mathrm{amp}}^{\mathrm{max}}$ are the limits within which $\mathrm{PRE}_{\mathrm{amp}}$ can vary, r_z^I is the inflection point (the distance from the bilayer center at which $\mathrm{PRE}_{\mathrm{amp}}$ is halfway between $\mathrm{PRE}_{\mathrm{amp}}^{\mathrm{min}}$ and $\mathrm{PRE}_{\mathrm{amp}}^{\mathrm{max}}$), and

SLOPE is a parameter which reports the steepness of the curve at the inflection point. The best fit (Fig. S6C) gave an adjusted coefficient of determination (R^2_{adj}) of 0.96, and was used to determine the position of the trimer structure with respect to the bilayer center ($r_z = 0$).

Generation of Env mutant constructs and production of monoclonal antibodies

Full-length Env mutants were generated using the 92UG037.8 gp160, described previously (10), as a template by QuikChange Site-Directed Mutagenesis (Agilent Technologies). All constructs were confirmed by restriction digestion and DNA sequencing. Anti-HIV-1 Env monoclonal antibodies and their Fab fragments were produced as described (10, 11). We have generated expression constructs of antibodies

PG9, PG16, PGT145, 2F5, 4E10 and 10E8 using synthetic genes made by GeneArt Gene Synthesis (Life Technologies, Carlsbad, CA) or GenScript. The DH570 expression constructs were kindly provided by Barton Haynes (Duke University); antibody VRC01 by John Mascola (VRC, NIH); the CHO stable line expressing antibody b6 by Dennis Burton (Scripps); 17b hybridoma by James Robinson (Tulane University); 3791 hybridoma by Susan Zolla-Pazner (New York University). The expression constructs of 10E8 were initially obtained from the NIH AIDS reagent program. Anti-His antibody MA1-21315 was purchased from ThermoFisher Scientific.

Antibody binding to the MPER-TMD in bicelles

The bicelle-reconstituted MPER-TMD trimer was examined for binding to several antibodies, including antigen binding fragment (Fab) of 2F5, 4E10, 10E8 and DH570, as well as a control Fab derived from an anti-His antibody MA1-21315. For binding to 2F5 or 4E10, the (^{15}N, 80% ^{2}H)-labeled MPER-TMD was reconstituted in bicelles with q = 0.5. For binding to the anti-His Fab, the (^{15}N, 80% ^{2}H)-labeled MPER-TMD with N-terminal 6His-tag reconstituted in the same bicelles was used. In all three cases, we mixed the MPER-TMD at 0.1 mM and Fab at 0.07 mM with a final molar ratio of 1.0:0.7. First, a reference 1D spectrum of the MPER-TMD before Fab addition was recorded at 600 MHz using a ^{15}N-edited TROSY-HSQC experiment. The same spectrum was then recorded at 2, 4, 6, and 8-hour time points after addition of Fab. Spectrum intensities at each time point relative to those of the reference spectrum were measured in the Bruker Topspin3.2 operating system using the multiple-spectra display mode. These intensities directly correlate to the fraction of the MPER-TMD in the NMR samples not bound to antibody. Hence, the fraction of the MPER-TMD in a conformation incompatible with Fab binding (Fraction Unbound), or equivalently, the fraction of the Fab unbound to the MPER-TMD, at various time points can be calculated as (I – 0.3) / (I_0 – 0.3), where I_0 is the

reference intensity set to 1, I is the fraction intensity relative to I_0 at a particular time, and subtraction of 0.3 was made to account for the 30% molar access of the MPER-TMD to the Fab. Linear fitting of the Fraction Unbound vs. Time points was performed using the *Origin* software (OriginLab, Northampton, MA) (Fig. 3G).

Production of pseudoviruses containing mutant Envs

Preparation of HIV-1 Env pseudoviruses containing mutations in the MPER, titration of pseudovirus stocks to determine the 50% tissue culture infectious dose per ml ($TCID_{50}$/ml) and the neutralization assay using TZM.bl cells were performed as previously described (1, 12).

HIV-1 p24 Antigen ELISA assay and Western blot

Viral stocks were boiled in a buffer containing 0.5% Triton X-100 for 60 min and analyzed for p24 antigen using a HIV-1 p24 antigen ELISA 2.0 kit (ZeptoMetrix Corporation, Buffalo, New York), as described (1). Western blots were carried out following our published protocol (1). Virus lysates were made by directly mixing p24-normalized virus stocks with Laemmli Sample Buffer (Bio-Rad, Hercules, CA) and boiling for 10 min. Lysates of cells expressing Env or its mutants were prepared by resuspending the cells in PBS (phosphate buffered saline) at a density of $2x10^6$ cells/ml, followed by treatment with the Sample Buffer and boiling for 10 min.

Flow cytometry

293T cells were transiently transfected with 2 μg of the 92UG037.8 gp160 expression construct or its MPER mutants. Flow cytometry was carried out as described(1, 10). All data were analyzed by FlowJo (FlowJo, LLC, Ashland, OR).

Cell-cell fusion assay

Cell-cell fusion assay, based on the α-complementation of E. coli β-galactosidase, was carried out as described previously (1). Briefly, 293T cells were cotransfected with either HIV-1 Env and the α fragment of β-galactosidase or CD4, CCR5 and the ω fragment of β-galactosidase. Env-expressing cells ($2.0x10^6$ cells/ml) were mixed with CD4- and CCR5-expressing cells ($2.0x10^6$ cells/ml). Cell-cell fusion was allowed to proceed at 37°C for 2 hr. Cell-cell fusion activity was quantified using a chemiluminescent assay system, Gal-Screen (Applied Biosystems, Foster City, CA).

Viral infectivity and antibody neutralization assays

Viral infectivity of HIV-1 92UG037.8 Env and the MPER mutants was measured by infecting TZM.bl cells with p24-normalized pseudovirus in growth media containing DEAE-dextran (11μg/ml). Luciferase activity of the reporter gene was quantified 48 hours post-infection, as previously described (13). Neutralization by monoclonal antibodies was also determined by the luciferase-based virus neutralization assay in TZM.bl cells (13). The assay measures the reduction in luciferase reporter gene expression in TZM-bl cells following a single round of virus infection. Briefly, 5-fold serial dilutions of antibody samples were performed in duplicate (96-well flat bottom plate) in 10% DMEM growth medium (100 μl/well). Virus was added to each well in a volume of 50 μl, and the plates were incubated for 1 hour at 37°C. TZM.bl cells were then added (1×10^4/well in 100 μl volume) in 10% DMEM growth medium containing DEAE-Dextran. Following a 48 hour incubation, luminescence was measured using Bright-Glo luciferase reagent (Promega, Madison, WI). Murine leukemia virus (MuLV) was used as a negative control virus for all assays. Antibodies used in this assay include IgG of b6, 3791, 17b, PG9, PG16, PGT145 and VRC01.

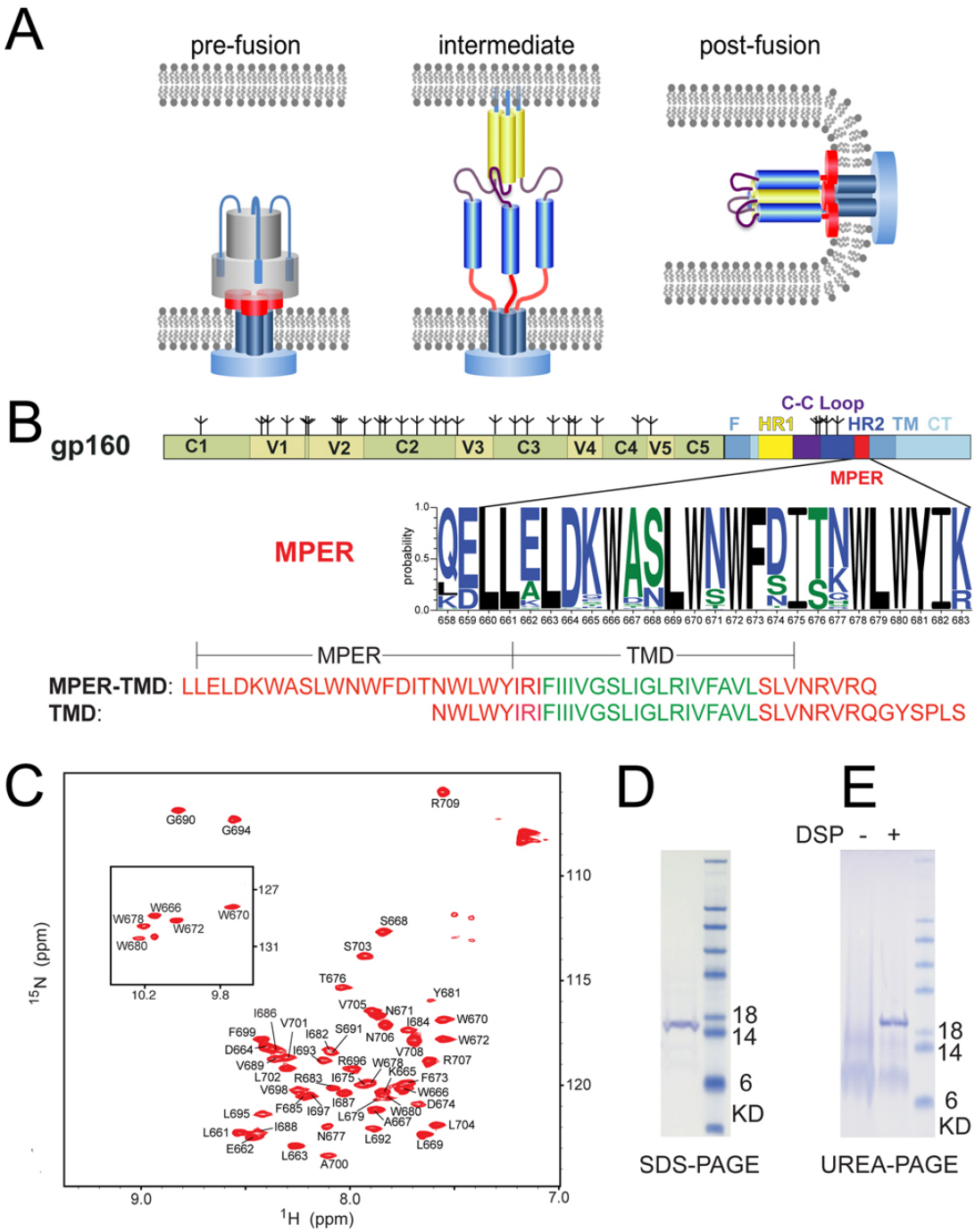
A
pre-fusion
intermediate
post-fusion
B
gp160
C1
V1
V2
C2
V3
C3
V4
C4
V5
C5
C-C Loop
F
HR1
HR2
TM
CT
MPER
MPER
probability
MPER
TMD
MPER-TMD: LLELDKWASLWNWFDITNWLWYIRIFIIIVGSLIGLRIVFAVLSLVNRVRQ
TMD: NWLWYIRIFIIIVGSLIGLRIVFAVLSLVNRVRQGYSPLS
C
D
E
DSP - +
18
14
6
KD
SDS-PAGE
UREA-PAGE

Figure S1. HIV-1 MPER and NMR sample preparation of the MPER-TMD in bicelles. (**A**) Schematic of HIV-1 gp41 in the pre-fusion, intermediate, and post-fusion states, with the MPER-TMD highlighted in red. (**B**) Schematic of HIV-1 gp160 with segments of gp120 and gp41 designated as follows: C1-C5, conserved regions 1-5; V1-V5, variable regions 1-5; F, fusion peptide; HR1, heptad repeat 1; C-C loop, the immunodominant loop with a disulfide bond; HR2, heptad repeat 2; MPER, membrane proximal external region; TM, transmembrane anchor; CT, cytoplasmic tail, and tree-like symbols, glycans. Sequence logos showing variations in the MPER (residues 660-683) among 5132 HIV-1 sequences with small residues in green, hydrophobic in black, and strongly polar or charged in blue (generated using ANALYZEALIGN of the Los Alamos National Laboratory). Amino acid sequences of the $gp41^{HIV1D(660-710)}$ (or MPER-TMD) construct used in the current study and the $gp41^{HIV1D(677-716)}$ (or TMD) construct in earlier study(1) showing the overlapped TM region (residues 683-704) of HIV-1 clade D isolate 92UG024.2. The TMD core which has essentially the same NMR chemical shifts in both constructs (residues 685-702) is shown in green; the MPER in red and the rest near the cytoplasmic tail in light blue. (**C**) Assigned NMR spectra of the MPER-TMD in bicelles. The ^{1}H-^{15}N TROSY-HSQC spectrum recorded at ^{1}H frequency of 750 MHz using (^{15}N, ^{2}H)-labeled protein. (**D**) SDS-PAGE of the MPER-TMD reconstituted in bicelles showing a homogeneous band at ~17 kDa position, consistent with the M.W. of a MPER-TMD trimer (~18.5 kDa). (**E**) Urea-PAGE analysis of crosslinking of an MPER-TMD mutant, K665R/D674K, in bicelles. We used standard, SDS-containing Laemmli buffers with a final urea concentration of 4.7M in the separating gel, 6.8M in the stacking gel, and 8M in the running buffer. The loading buffer was 9.6M in urea, 3 % in SDS, and 5% in glycerol before mixing (25 μL plus 5 μL sample) with protein sample and boiling. The uncrosslinked sample ran as a diffuse band near the position expected for a monomer (lane 1), whereas the mutant crosslinked by DSP ran as a sharp band at the position expected for a trimer (~20 kDa including DSP) (lane 2). The mutations were designed retrospectively from examination of the structure, to enhance crosslinking efficiency (see SI Methods).

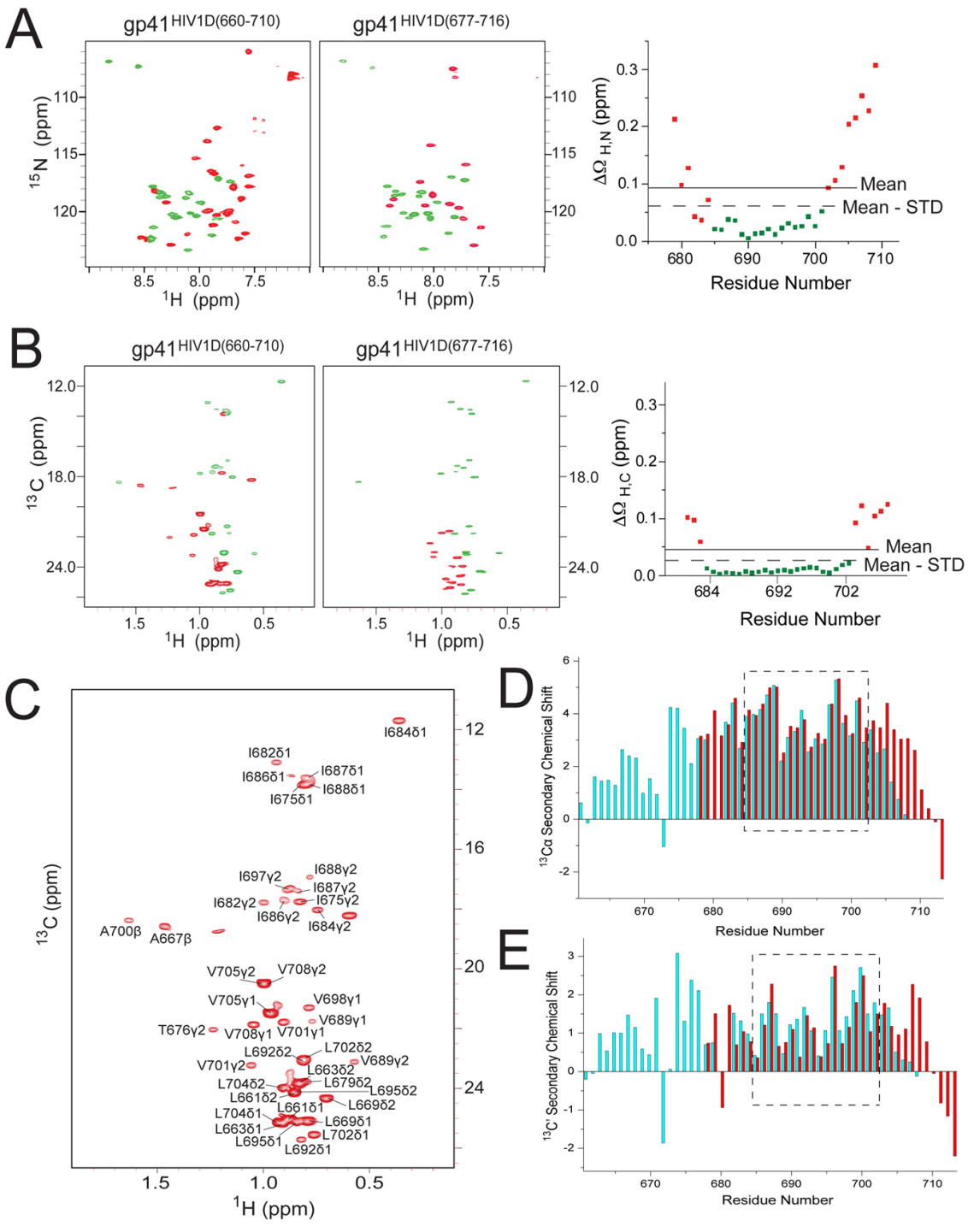
A
gp41 HIV1D(660-710)
gp41 HIV1D(677-716)
15N (ppm)
1H (ppm)
ΔΩ H,N (ppm)
Mean
Mean - STD
Residue Number
B
gp41 HIV1D(660-710)
gp41 HIV1D(677-716)
13C (ppm)
1H (ppm)
ΔΩ H,C (ppm)
Mean
Mean - STD
Residue Number
C
I684δ1
I682δ1
I686δ1
I687δ1
I688δ1
I675δ1
I697γ2
I688γ2
I687γ2
I682γ2
I675γ2
I686γ2
I684γ2
A700β
A667β
V705γ2
V708γ2
V705γ1
V698γ1
V689γ1
T676γ2
V708γ1
V701γ1
L692δ2
L702δ2
V701γ2
V689γ2
L663δ2
L704δ2
L679δ2
L695δ2
L661δ2
L661δ1
L669δ2
L704δ1
L669δ1
L663δ1
L702δ1
L695δ1
L692δ1
13C (ppm)
1H (ppm)
D
13Cα Secondary Chemical Shift
Residue Number
E
13C' Secondary Chemical Shift
Residue Number

Figure S2. NMR resonances of the MPER-TMD of HIV-1 gp41 in bicelles. (**A**) ^{1}H-^{15}N TROSY-HSQC spectra of the MPER-TMD (left) and TMD (right) displayed in the color scheme of (Fig. S1B), showing that the TMD cores of the two constructs have the same resonance shifts (green). The spectra were recorded with MPER-TMD and TMD samples, reconstituted in DMPC/DHPC bicelles (q = 0.5) in the same way as described in the SI Methods. The right-most panel shows the normalized chemical shift difference, $\Delta\Omega_{H,N}$ (Supplementary Methods), between the two spectra for each of the overlapping residues. The solid and dashed lines represent the mean $\Delta\Omega_{H,N}$ and mean $\Delta\Omega_{H,N}$ – standard deviation of $\Delta\Omega_{H,N}$, respectively. The error of $\Delta\Omega_{H,N}$, estimated based on peak line-width and signal/noise ratio, are all less than 0.0015 ppm and are thus not visible in the plot. (**B**) The methyl group chemical shift differences between the ^{1}H-^{13}C HSQC spectra of the MPER-TMD (left) and TMD (right) constructs, displayed in the same manner as in (A). The residue number labels in the $\Delta\Omega_{H,C}$ plot are approximations, as there is not a methyl group for every residue. **(C)** Assigned methyl group resonances of the MPER-TMD in bicelles. The ^{1}H-^{13}C HSQC (28 ms ^{13}C constant time) recorded at ^{1}H frequency of 800 MHz using (^{15}N, ^{13}C)-labeled protein, showing the assignments of the methyl group resonances. The proteins were reconstituted in DMPC/DHPC bicelles (q = 0.5), in which the acyl chains of DMPC and DHPC were deuterated. (**D** and **E**) Comparison of the ^{13}Cα and ^{13}C' secondary chemical shifts, respectively, between the gp41$^{HIV1D(660-710)}$ (cyan) and the gp41$^{HIV1D(677-716)}$ (red) reconstituted in bicelles. The secondary chemical shift values were generated using the program TALOS+ (6). The boxed region is the core region of the TMD including residues 685-702.

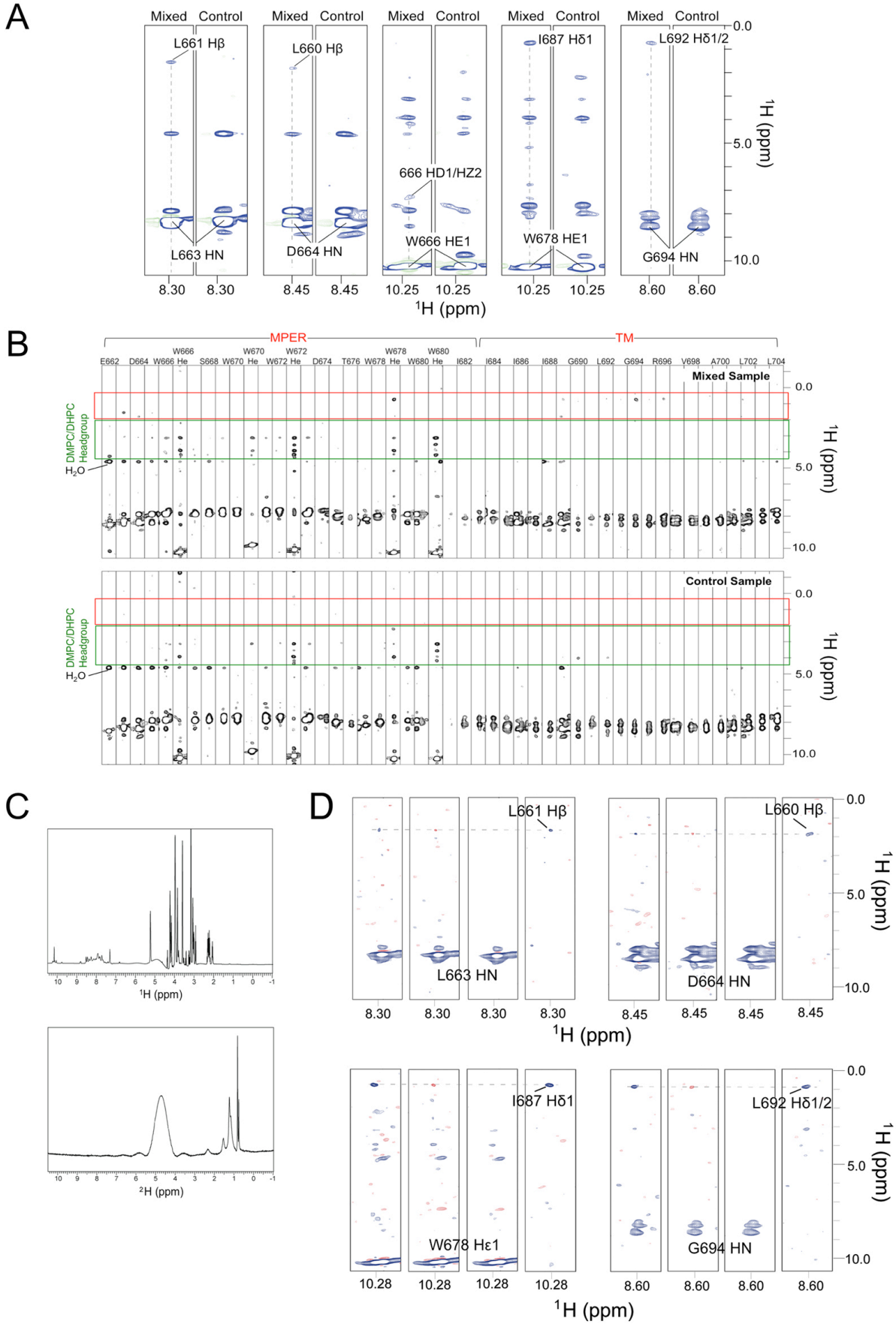
A
Mixed
Control
L661 Hβ
L660 Hβ
I687 Hδ1
L692 Hδ1/2
L663 HN
D664 HN
666 HD1/HZ2
W666 HE1
W678 HE1
G694 HN
8.30
8.45
10.25
8.60
0.0
5.0
10.0
¹H (ppm)
B
MPER
TM
E662 D664 W666 W666 He S668 W670 W670 He W672 W672 He D674 T676 W678 W678 He W680 W680 He I682 I684 I686 I688 G690 L692 G694 R696 V698 A700 L702 L704
Mixed Sample
Control Sample
DMPC/DHPC Headgroup
H2O
C
¹H (ppm)
²H (ppm)
D
L661 Hβ
L660 Hβ
L663 HN
D664 HN
I687 Hδ1
L692 Hδ1/2
W678 Hε1
G694 HN
10.28
8.60
8.45
8.30

Figure S3. Inter-protomer NOEs for the MPER. (**A**) Example strips from 3D ^{15}N-edited NOESY-TROSY-HSQC (τ_{NOE} = 200 ms) spectra recorded using an isotopically mixed sample (left strips) and a control sample (right strips). The mixed sample consists of 0.4 mM (^{15}N, ^{2}H)-labeled MPER-TMD and 0.4 mM (15% ^{13}C)-labeled MPER-TMD, premixed at the cell level before cell lysis and protein purification. The control sample contains only 0.4 mM (^{15}N, ^{2}H)-labeled MPER-TMD. The spectra were recorded at ^{1}H frequency of 800 MHz. The inter-protomer NOE crosspeaks between amides and aliphatic protons due to isotope mixing are labeled. (**B**) Essentially complete NOE strips from the mixed and control samples. In panels **A** and **B**, the NOEs must have ^{1}H chemical shift > 0.3ppm, but those with ^{1}H chemical shift between 2 and 4.4ppm (green box) might have come from the protons of the DMPC/DHPC headgroups, which were not deuterated in our sample (only the acyl chains were perdeuterated). Although some appeared to be inter-chain NOEs, we chose not to use them, leaving a chemical shift region between 0.3 and 2ppm (red box), within which most of the inter-chain NOEs were identified. The ^{15}N, ^{2}H labeled protein used for the mixed and control samples were from the same batch of expressing cells. Had the NOEs assigned as intermolecular been from site-specific ^{1}H contamination, they would also have appeared in the spectrum of the control sample. (**C**) 1D NMR spectra of the sample used for recording the reference NOE spectrum. In this sample, the MPER-TMD is (^{15}N, ^{2}H) labeled, and the acyl chains of DMPC and DHPC are perdeuterated. The left spectrum is a 1D ^{1}H spectrum, showing essentially no signals < 2 ppm. The right spectrum is a 1D ^{2}H spectrum, showing that the methylene and methyl groups in the sample are ^{2}H labeled. (**D**) Mixed NOE experiment with J(^{13}C-^{1}H) modulation. See Methods. Strips from 3D ^{15}N-edited NOESY-TROSY-HSQC (τ_{NOE} = 200 ms) spectra recorded using an isotopically mixed sample that contained 0.8 mM MPER-TMD, as a 50:50 mixture of (^{15}N, ^{2}H)-labeled MPER-TMD and (^{13}C, ^{1}H)-labeled MPER-TMD. Two interleaved 3D spectra were recorded with ^{1}H-^{13}C J evolution introduced before the NOE mixing (J^{evol1} = 0 ms, J^{evol2} = 8 ms). For each NOE pair, four panels are shown: Spectrum1 (with positive inter-NOEs, blue), Spectrum2 (with negative inter-NOEs, red), Summation of spectra 1 & 2 (inter-NOE peaks canceled), and Subtraction of spectra 1 & 2 (inter-NOE peaks enhanced and other peaks canceled). Upper left: NOEs between L663^{HN} and L661$^{H\beta}$; upper right: NOEs between D664^{HN} and L660$^{H\beta}$; lower left: NOEs between W678$^{H\varepsilon1}$ and I687$^{H\delta1}$; lower right: NOEs between G694^{HN} and L692$^{H\delta1/2}$.

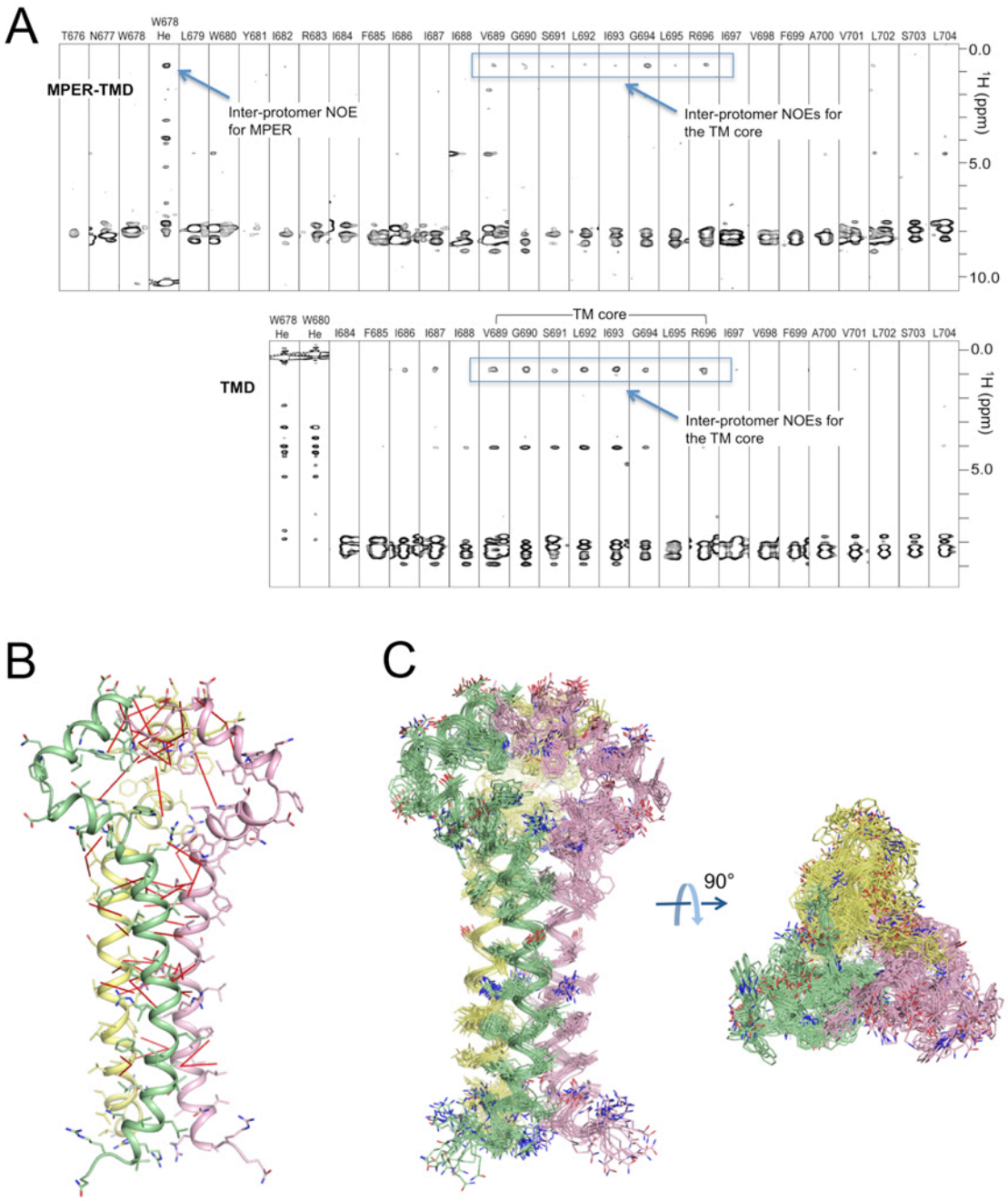

Figure S4. MPER-TMD and TMD alone. (**A**) Comparison of inter-protomer, TM-core NOEs for the MPER-TMD and the TMD samples. The NOE spectrum of the TMD sample was taken from Figure S5 of Dev J, *et al.* (2016). *Science* 353:172-175 (1). Reprinted with permission of AAAS. (**B**) Ribbon representation of the trimer structure showing NOE-derived intermonomer restraints (red lines). (**C**) Ensemble of 15 lowest energy structures calculated using NMR-derived structural restraints (Table S1). Structures are shown as thin ribbon representation of the backbones and stick representation of the side chains.

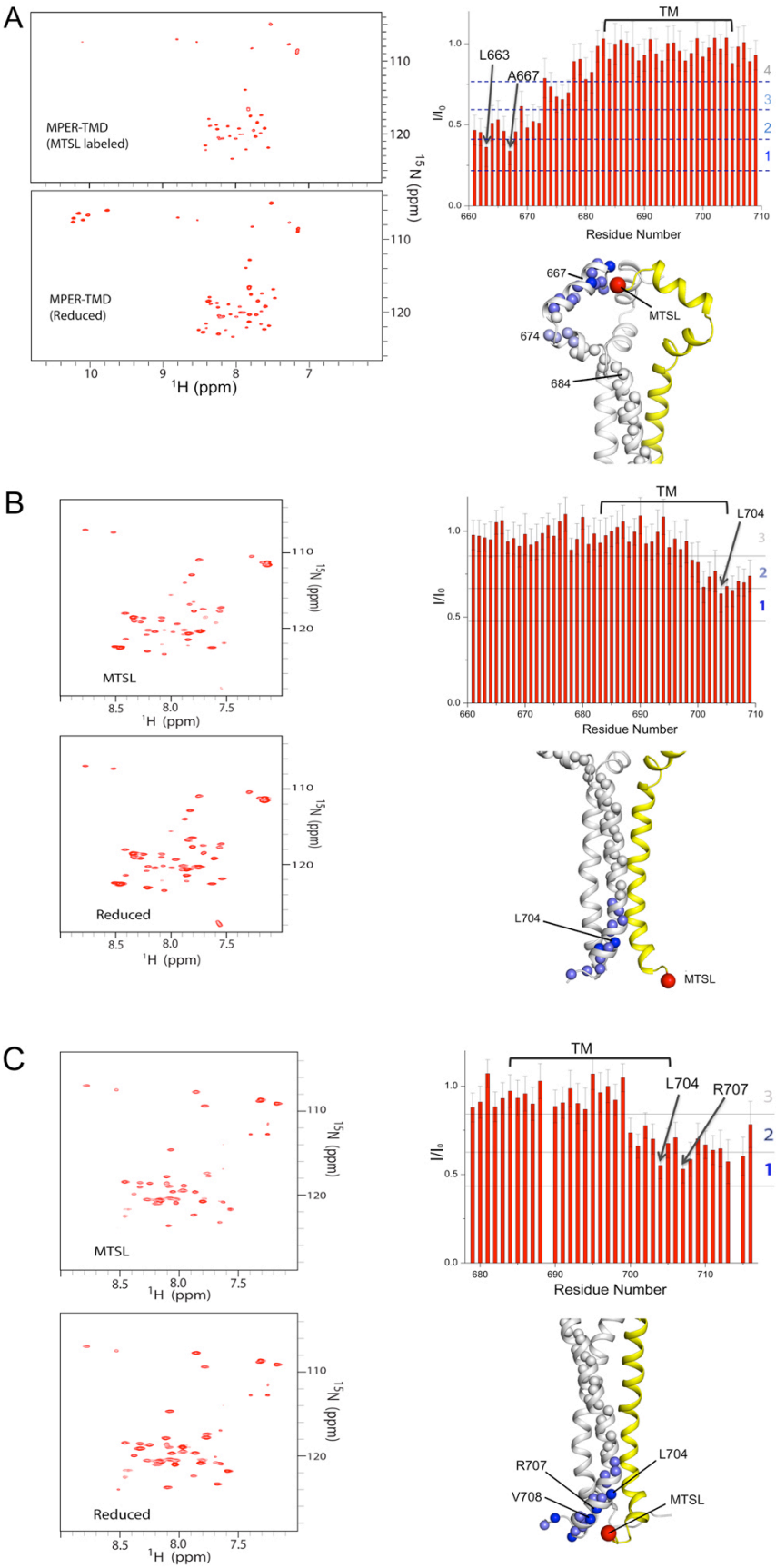
A
MPER-TMD
(MTSL labeled)
MPER-TMD
(Reduced)
^{15}N (ppm)
^{1}H (ppm)
TM
L663
A667
I/I$_0$
Residue Number
667
MTSL
674
684
B
MTSL
Reduced
L704
C
R707
V708

Figure S5. Mixed PRE data for the MPER-TMD and the TMD: both form homogeneous oligomers. The samples consist of ~1:1 ratio of (^{15}N, ~70% ^{2}H) labeled protein and unlabeled protein with MTSL near either the N- or the C-terminus of the construct, reconstituted in bicelles with $q \approx 0.5$. (**A**) Mixed PRE data for the MPER-TMD with MTSL labeled at position 660. *Left*: ^{1}H-^{15}N TROSY-HSQC spectra of the sample before (top) and after (bottom) the addition of 10 mM sodium ascorbate. *Top Right*: Residue-specific PRE, defined as the ratio of intensity before (I) and after (I_0) reducing with ascorbate. Regions between the dashed lines are defined as different PRE ranges. *Bottom Right*: A structural view showing the positions of backbone amide protons (spheres) that show strong PRE. Ribbon representations of the ^{15}N and MTSL labeled strands are shown in gray and yellow, respectively. The MTSL position is indicated by the red sphere. The amide protons are colored according to the PRE ranges defined in the top right panel. (**B**) Mixed PRE data for the MPER-TMD with MTSL labeled at position 710, presented in the same arrangement as in A. (**C**) Mixed PRE data for the TMD (residues 677-716) with MTSL labeled at position 716, presented in the same arrangement as in A.

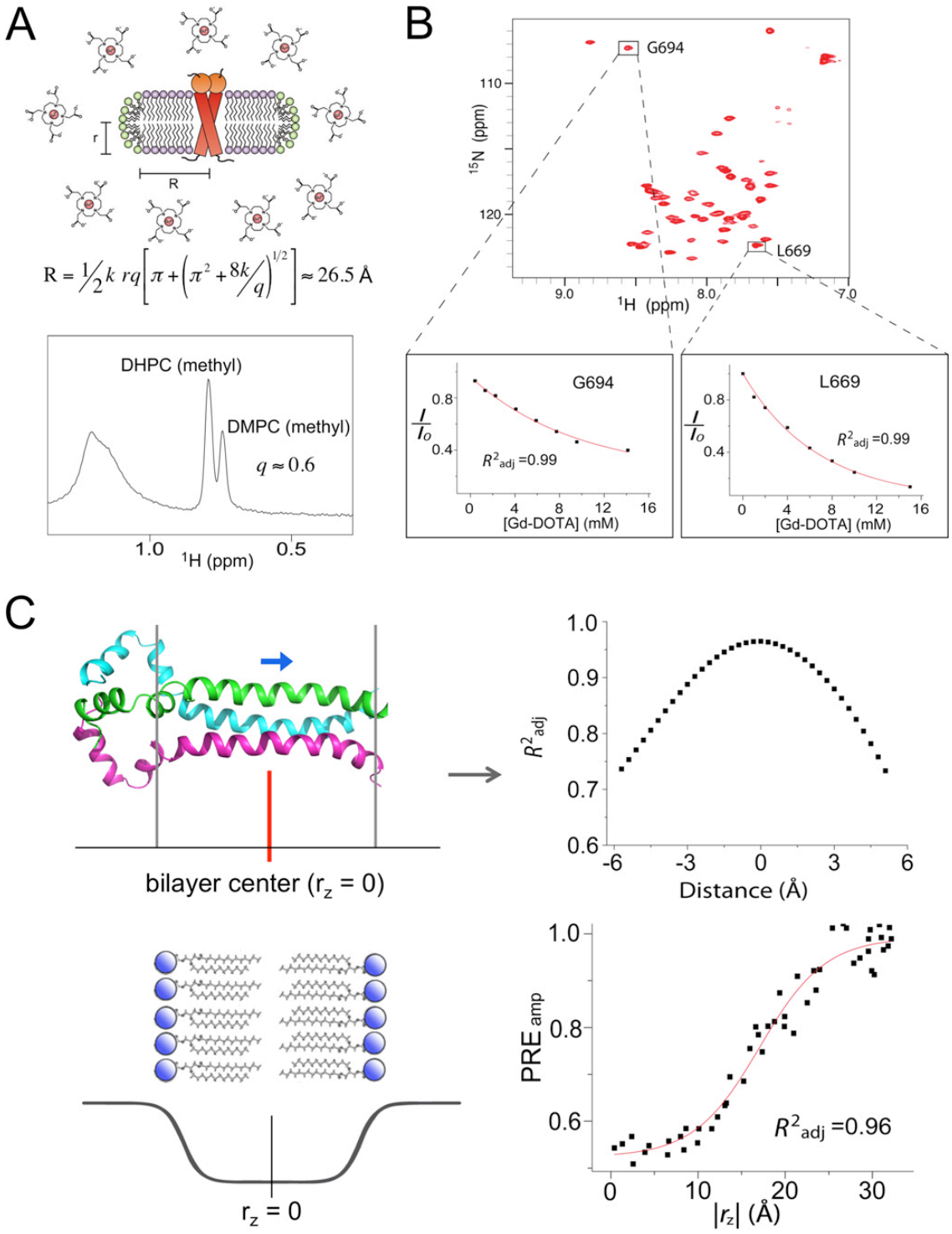
A
r
R
$R = \frac{1}{2} k\, rq\left[\pi + \left(\pi^2 + 8k/q\right)^{1/2}\right] \approx 26.5$ Å
DHPC (methyl)
DMPC (methyl)
$q \approx 0.6$
1.0
0.5
^{1}H (ppm)
B
G694
L669
110
120
^{15}N (ppm)
9.0
8.0
7.0
^{1}H (ppm)
G694
L669
$\frac{I}{I_o}$
0.8
0.4
R^2_{adj} =0.99
0
4
8
12
16
[Gd-DOTA] (mM)
C
bilayer center (r_z = 0)
r_z = 0
1.0
0.9
0.8
0.7
0.6
R^2_{adj}
-6
-3
0
3
6
Distance (Å)
PRE amp
1.0
0.8
0.6
R^2_{adj} =0.96
0
10
20
30
$|r_z|$ (Å)

Figure S6. **Solvent PRE analysis for characterizing membrane partition of the MPER-TMD**. (**A**) Diagram illustrating titration of the bicelle-reconstituted MPER-TMD with Gd-DOTA (upper panel). The radius of the bilayer region of the bicelle (*R*) is given by the equation (14, 15) below the drawing, where *r* is the radius of the DHPC rim (20 Å), *q* is the molar ratio of DMPC to DHPC (0.6), and *k* is the ratio of the head group area of DMPC to that of DHPC (0.6). Lower panel is the 1D ^{1}H spectrum of the bicelle sample recorded at 600 MHz, showing that the peak intensity ratio of the DMPC terminal methyl groups to that of the DHPC terminal methyl groups is 0.6 (or $q = 0.6$). (**B**) PRE vs. [Gd-DOTA] for L669 and G694, measured with a series of ^{1}H-^{15}N TROSY-HSQC spectra recorded at various Gd-DOTA concentrations. The data were fitted to the exponential decay function (Eq. 1 in Methods) to determine the PRE amplitude (PREamp). The PRE is defined as the ratio of peak intensity in the presence (I) and absence (I_0) of Gd-DOTA. The PREamp vs. residue number is shown in Fig. 2A. (**C**) Assignment of the bilayer center to the MPER-TMD by data fitting. Left: Illustration for sliding the MPER-TMD along the 3-fold axis (or bilayer normal) to yield best fit to the symmetric sigmoidal function (Eq. 2 in SI Methods). The $r_z = 0$ of the sigmoidal function corresponds to the bilayer center. Right upper: The adjusted coefficient of determination (R^2_{adj}) from data fitting versus deviation from the true bilayer center. The plot shows that R^2_{adj} is a reliable indicator of the protein position with an error of about ± 0.3 Å. Right lower: The best fit of the PREamp vs. r_z data to the symmetric sigmoidal function. The same fit is shown in Fig. 2B.

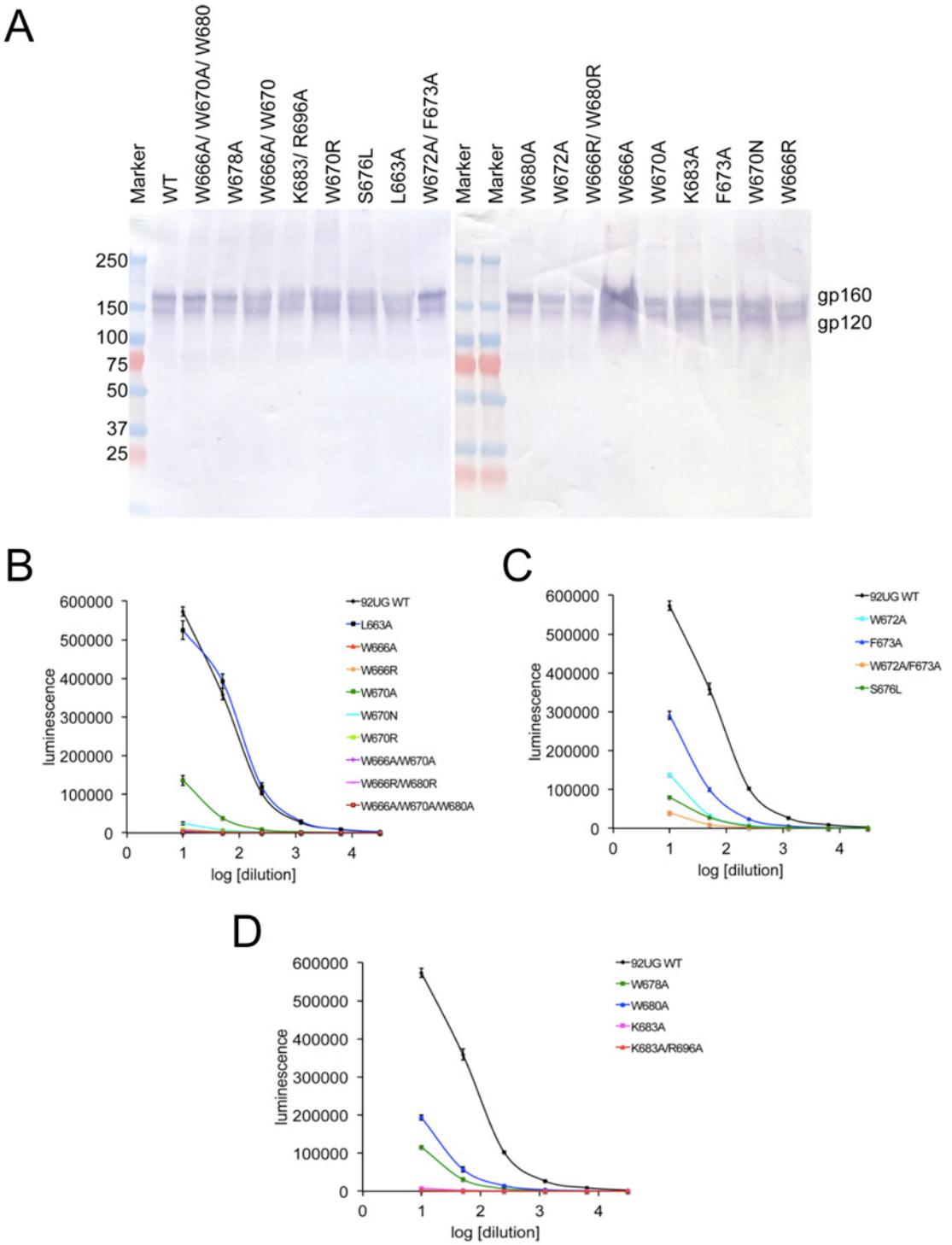
A
Marker
WT
W666A/ W670A/ W680
W678A
W666A/ W670
K683/ R696A
W670R
S676L
L663A
W672A/ F673A
Marker
Marker
W680A
W672A
W666R/ W680R
W666A
W670A
K683A
F673A
W670N
W666R
250
150
100
75
50
37
25
gp160
gp120
B
600000
500000
400000
300000
200000
100000
0
luminescence
0
1
2
3
4
log [dilution]
92UG WT
L663A
W666A
W666R
W670A
W670N
W670R
W666A/W670A
W666R/W680R
W666A/W670A/W680A
C
600000
500000
400000
300000
200000
100000
0
luminescence
0
1
2
3
4
log [dilution]
92UG WT
W672A
F673A
W672A/F673A
S676L
D
600000
500000
400000
300000
200000
100000
0
luminescence
0
1
2
3
4
log [dilution]
92UG WT
W678A
W680A
K683A
K683A/R696A

Figure S7. Viral infectivity of Env mutants. (**A**) Incorporation of Env mutants into pseudoviruses analyzed by western blot. Env samples prepared from p24-normalized pseudoviruses containing either HIV-1 gp92UG037.8 Env or each of its MPER mutants were detected by an anti-V3 antibody 3791. (**B-D**) Viral infectivity**.** Pseudoviruses containing Env MPER mutants were normalized by p24-antigen, titrated 10 times using 5-fold dilution series, and tested for viral infectivity in TZM.bl cells. The Env mutants are grouped in (**B**) for those containing mutations in the hydrophobic core; in (**C**) containing mutations in the turn; and in (**D**) containing mutations in the kink. The experiment was carried out in quadruplicate. Error bars indicate the standard deviation calculated by Excel.

A

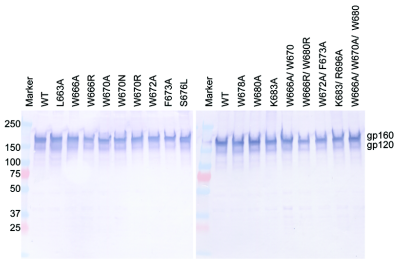

C

Mutation	Mean Fluorescence Intensity (MFI)		
	2G12	VRC01	PG16
WT	1254	820	648
L663A	1482	960	737
W666A	578	395	237
W666R	1044	794	351
W670A	1214	918	526
W670N	1039	776	400
W670R	505	347	222
W672A	820	805	454
F673A	1124	893	574
T676L	930	641	383
W678A	1099	841	497
W680A	1011	755	496
K683A	711	517	243
W666A/W670A	736	494	288
W666R/W680R	867	649	371
W672A/F673A	1374	1169	454
K683A/ R696A	930	715	301
W666A/W670A/W680A	910	646	347
293T	21	10	10

B

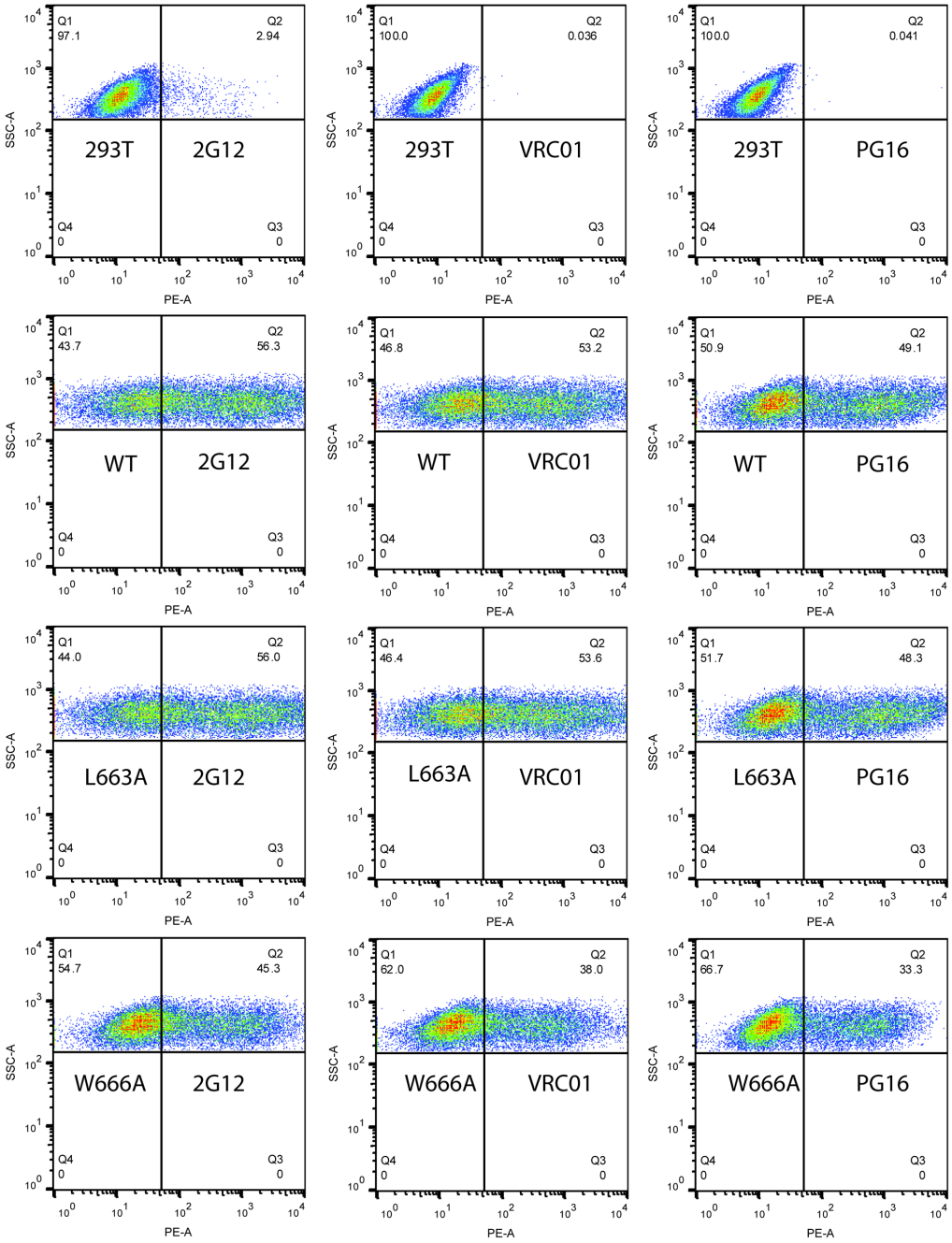

Figure S8. Expression and cell-cell fusion of HIV-1 Env and its MPER mutants.

(A-C)

(**A**) Expression and processing of Env mutants expressed in 293T cells. Env samples prepared from 293T cells transiently transfected with 1 μg of the HIV-1 gp92UG037.8 gp160 expression plasmid or each of MPER mutants were detected by an anti-V3 antibody 3791.

(**B**) Cell-surface expression of Env mutants detected by flow cytometry. Representative dot plots for negative control 293T cells, cells expressing the wildtype Env (WT), or mutants L663A and W666A, measured by flow cytometry using monoclonal antibodies 2G12, VRC01 and PG16.

(**C**) Summary of mean fluorescence intensity (MFI) from data shown in (B) for the wildtype and 17 MPER mutants, as well as for the 293T cell control.

D

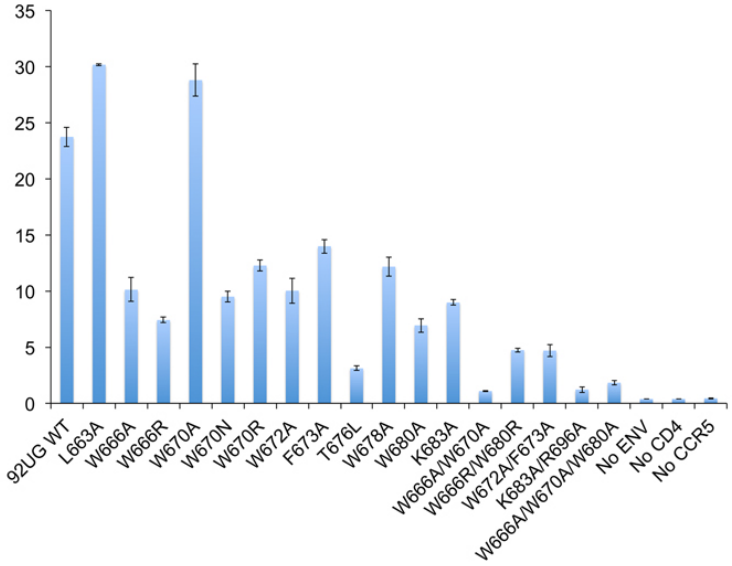

E

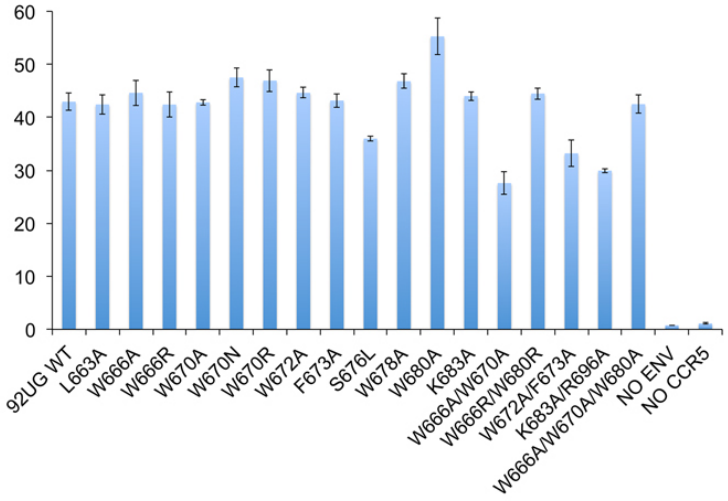

F

Mutation	Structural element	Viral infectivity[a]	Cell-cell fusion[b] (low Env level)	Cell-cell fusion (high Env level)
WT	n/a	100.0±2.1	100.0±3.6	100.0±3.9
L663A	hydrophobic core	91.5±4.2	127.1±0.4	98.8±4.3
W666A		0.3±0.1	42.6±1.9	103.9±5.8
W666R		0.4±0.1	31.2±0.3	98.7±5.4
W670A		23.7±2.3	121.3±7.4	99.7±1.2
W670N		4.3±0.7	40.0±0.8	110.6±4.5
W670R		1.6±0.1	51.7±1.0	109.3±5.3
W666A/W670A		0.8±0.1	4.6±0.0	64.3±3.2
W666R/W680R		1.2±0.0	19.9±0.1	103.6±2.6
W666A/W670A/W680A		0.6±0.0	7.7±0.1	98.9±4.0
W672A	turn	24.2±0.6	42.3±2.0	103.9±2.4
F673A		50.8±1.9	58.9±1.5	100.5±3.0
W672A/F673A		6.9±0.3	19.8±0.5	77.3±4.4
S676L		13.9±0.5	13.1±0.1	83.8±1.0
W678A	kink	20.2±0.5	51.3±1.8	109.0±3.5
W680A		33.7±1.1	29.2±0.7	128.7±10.5
K683A		1.4±0.2	37.8±0.4	102.5±2.0
K683A/R696A		0.3±0.0	5.2±0.1	69.7±0.7

Figure S8. Expression and cell-cell fusion of HIV-1 Env and its MPER mutants.

(D-F)

(**D**) Cell-cell fusion of HIV-1 Env and its MPER mutants at a low expression level. 293T cells transfected with 75 ng of the 92UG037.8 Env expression plasmid or each of its TMD mutants were mixed with CD4- and CCR5-expressing cells. Cell-cell fusion led to reconstitution of active β-galactosidase; fusion activity was quantified by a chemiluminescent assay. No Env, no CD4 and no CCR5 were negative controls. The experiment was carried out in triplicate and repeated at least twice with similar results. Error bars indicate the standard deviation calculated by the Excel STDEV function. Data points are means ± standard deviations from triplicate measurements. The data are also summarized in Fig. S8F.

(**E**) Cell-cell fusion of HIV-1 Env and its MPER mutants at a high expression level. 293T cells transfected with 10 μg of the 92UG037.8 Env expression plasmid or each of its MPER mutants were fused with CD4- and CCR5-expressing cells. No Env, no CCR5 were negative controls. The experiment was carried out in triplicate and repeated at least twice with similar results. Error bars indicate the standard deviation calculated by the Excel STDEV function. Data points are means ± standard deviations from triplicate measurements.

(**F**) Functional analysis of mutations in the HIV-1 TMD. [a] Viral infectivity was determined using p24-normalized pseudoviruses; titration data for each virus with 5-fold dilution series are also shown in Fig. S7B-D. [b] Cell-cell fusion assay was performed at both high and low Env expression levels, as displayed in panels **D** and **E**.

Table S1. NMR and refinement statistics

NMR distance and dihedral constraints [a]	MPER (660-683)	TM (684-710)
Distance constraints from NOE [b]	282	432
Short-range intramolecular ($\|i-j\| \leq 4$)	237	390
Long-range intramolecular ($\|i-j\| \geq 5$)	21	0
Intermolecular	24	42
Total dihedral angle restraints [c]	252	
ϕ (TALOS)	126	
ψ (TALOS)	126	
Structure statistics [d]		
Violations (mean ± s.d.)		
Distance constraints (Å)	0.155 ± 0.008	
Dihedral angle constraints (º)	1.281 ± 0.095	
Deviations from idealized geometry		
Bond lengths (Å)	0.032 ± 0.000	
Bond angles (º)	1.641 ± 0.019	
Impropers (º)	0.931 ± 0.039	
Average pairwise r.m.s. deviation (Å) [e]		
Heavy	1.714	
Backbone	1.192	

[a] The numbers of constraints are summed over all three subunits.

[b] For the MPER, all NOE restraints were obtained in the current study. For the TM, the NOE restraints for residues 685 – 701 (total 204) were taken from our earlier NMR study of the TMD, and the rest were obtained in the current study.

[c] Backbone ϕ and ψ restraints and their respective uncertainties were obtained from the "GOOD" dihedrals generated by the TALOS+ program (6) based on the backbone chemical shift values.

[d] Statistics are calculated and averaged over an ensemble of the 15 lowest energy structures out of 150 calculated structures.

[e] The precision of the atomic coordinates is defined as the average r.m.s. difference between the 15 final structures and their mean coordinates.

References

1. Dev J, *et al.* (2016) Structural basis for membrane anchoring of HIV-1 envelope spike. *Science* 353(6295):172-175.
2. Delaglio F, *et al.* (1995) NMRPipe: a multidimensional spectral processing system based on UNIX pipes. *J. Biomol. NMR* 6:277-293.
3. Bartels C, Xia TH, Billeter M, Guntert P, & Wuthrich K (1995) The program XEASY for computer-supported NMR spectral analysis of biological macromolecules. *Journal of biomolecular NMR* 6(1):1-10.
4. Salzmann M, Wider G, Pervushin K, & Wuthrich K (1999) Improved sensitivity and coherence selection for [15N,1H]-TROSY elements in triple resonance experiments. *Journal of biomolecular NMR* 15(2):181-184.
5. Szyperski T, Neri D, Leiting B, Otting G, & Wuthrich K (1992) Support of 1H NMR assignments in proteins by biosynthetically directed fractional 13C-labeling. *Journal of biomolecular NMR* 2(4):323-334.
6. Shen Y, Delaglio F, Cornilescu G, & Bax A (2009) TALOS+: a hybrid method for predicting protein backbone torsion angles from NMR chemical shifts. *Journal of biomolecular NMR* 44(4):213-223.
7. Schwieters CD, Kuszewski JJ, Tjandra N, & Clore GM (2003) The Xplor-NIH NMR molecular structure determination package. *Journal of magnetic resonance* 160(1):65-73.
8. Chiliveri SC, Louis JM, Ghirlando R, Baber JL, & Bax A (2018) Tilted, Uninterrupted, Monomeric HIV-1 gp41 Transmembrane Helix from Residual Dipolar Couplings. *J Am Chem Soc* 140(1):34-37.
9. Piai A, Fu Q, Dev J, & Chou JJ (2017) Optimal Bicelle Size q for Solution NMR Studies of the Protein Transmembrane Partition. *Chemistry* 23(6):1361-1367.
10. Chen J, *et al.* (2015) HIV-1 ENVELOPE. Effect of the cytoplasmic domain on antigenic characteristics of HIV-1 envelope glycoprotein. *Science* 349(6244):191-195.
11. Kovacs JM, *et al.* (2012) HIV-1 envelope trimer elicits more potent neutralizing antibody responses than monomeric gp120. *Proc Natl Acad Sci U S A* 109(30):12111-12116.
12. Li M, *et al.* (2005) Human immunodeficiency virus type 1 env clones from acute and early subtype B infections for standardized assessments of vaccine-elicited neutralizing antibodies. *J Virol* 79(16):10108-10125.
13. Sarzotti-Kelsoe M, *et al.* (2014) Optimization and validation of the TZM-bl assay for standardized assessments of neutralizing antibodies against HIV-1. *J Immunol Methods* 409:131-146.
14. Sanders CR, 2nd & Schwonek JP (1992) Characterization of magnetically orientable bilayers in mixtures of dihexanoylphosphatidylcholine and dimyristoylphosphatidylcholine by solid-state NMR. *Biochemistry* 31(37):8898-8905.
15. Glover KJ, *et al.* (2001) Structural evaluation of phospholipid bicelles for solution-state studies of membrane-associated biomolecules. *Biophysical journal* 81(4):2163-2171.